energies

MDPI

Review

Research Progress and Prospects of Multi-Stage Centrifugal Pump Capability for Handling Gas–Liquid Multiphase Flow: Comparison and Empirical Model Validation

Asad Ali [1], Jianping Yuan [1], Fanjie Deng [1], Biaobiao Wang [1], Liangliang Liu [2], Qiaorui Si [1,*] and Noman Ali Buttar [3]

1   National Research Center of Pumps, Jiangsu University, Zhenjiang 212013, China; 5103190316@stmail.ujs.edu.cn (A.A.); yh@ujs.edu.cn (J.Y.); 2221811005@stmail.ujs.edu.cn (F.D.); wbbujs@163.com (B.W.)
2   Shanghai Kaiquan Pump Co., Ltd., Cao'an Road, Jiading, Shanghai 201800, China; liuliangliang@kaiquan.com.cn
3   School of Agricultural Engineering, Jiangsu University, Zhenjiang 212013, China; noman_buttar@yahoo.com
*   Correspondence: siqiaorui@ujs.edu.cn; Tel.: +86-136-5529-3881

Abstract: The working capability of multi-stage pumps, such as electrical submersible pumps (ESPs) handling multiphase flow, has always been a big challenge for petroleum industries. The major problem is associated with the agglomeration of gas bubbles inside ESP-impellers, causing pump performance degradation ranging from mild to severe deterioration (surging/gas pockets). Previous literature showed that the two-phase performance of ESPs is greatly affected by gas involvement, rotational speed, bubble size, and fluid viscosity. Thus, it is necessary to understand which parameter is actually accountable for performance degradation and different flow patterns in ESP, and how it can be controlled. The present study is mainly focused on (1) the main parameters that impede two-phase performance of different ESPs; (2) comparison of existing empirical models (established for two-phase performance prediction and surging initiation) with our single-stage centrifugal pump results to determine their validity and working-range; (3) gas-handling techniques applied to enhance the multiphase performance of ESPs. Firstly, it aims at understanding the internal flow mechanism in different ESP designs, followed by test studies based on empirical models, visualization techniques, bubble-size measurements, and viscosity analysis. The CFD-based (computational fluid dynamics) numerical analysis concerning multiphase flow is described as well. Furthermore, gas-handling design methods are discussed that are helpful in developing the petroleum industry by enhancing the multiphase performance of ESPs.

Keywords: multiphase flow; empirical models; computational fluid dynamics; petroleum industries; gas-handling techniques; electrical submersible pumps; flow visualization; viscosity analysis

1. Introduction

The submersible pump, since its inception in 1910 by Russian engineer, Armais Arutunoff [1,2], has had a great impact in oil and gas industries. These downhole pumps are used to convert kinetic energy into hydraulic pressure head and exhibit high efficiency. Globally, the electrical submersible pump (ESP) systems are the second most extensively applied for artificial lift and are used in more than 90 percent of the oil production wells and high-volume production [3–5]. ESP performance is affected by many factors including gas involvement, rotational speed, bubble size, fluid density and viscosity [6,7]. When handling two-phase flow—gas and liquid—the involvement of gas and bubble size distribution can cause pump performance degradation, ranging from mild deterioration to severe deterioration (surging and gas-pocket formation), and finally may result in complete flow blocking (gas locking) [8,9]. The surging, which is related to gas-pocket formation [10,11],

can cause vibrations and reduce the working capability of the pump, while the gas pocket can seriously affect the liquid production rate [12].

Numerous studies have been conducted regarding the gas-handling ability of the ESP system since late 1980s, and several ESP design models are available that are able to sustain up to 95% of the free gas, using helico-axial pumps [13] and gas separators [14]. As the removal of free gas from the gas–liquid mixture is not always successful and because the axial pumps have high manufacturing cost and exhibit low pressure rise compared to traditional models, the gas-handling ability of the ESP is a big issue for the petroleum industry. In order to design a pump that can produce a higher head and higher efficiency while handling gas, it needs its performance to be described in two-phase flow conditions. Although the study of two-phase flow has become common for ESPs, the internal flow behavior, the formation of bubble and its breakup phenomena are not yet fully understood. Even the use of the flow visualization technique for examining the internal flow behavior, including bubble inception, bubble size, and bubble motion [15–17], is complicated due to the complex geometry of the ESP. Thus, we need to deepen the understanding of the mixed-flow mechanism in designing the multi-stage ESPs that can handle gas in a better way.

The present paper is a comprehensive review of recent research progresses regarding experimental and numerical analysis on the gas-handling ability of ESP under multiphase flow conditions. This review provides a better understanding of the complex flow behavior inside the rotating impeller of ESP, and reports some design methods that have increased the gas–liquid two-phase flow-handling ability of ESP. Section 2 focuses on the flow mechanism inside ESP in terms of velocity triangles and the Euler equation. The types of ESP and their capabilities in handling gas in multiphase flow are also discussed. Section 3 presents an experimental analysis in which the hydraulic performance and gas-handling ability of ESPs using empirical correlations, flow visualization, void fraction distribution and bubble size measurements in two-phase flow are discussed. Then, in Section 4, two-phase flow performances of ESPs are described on the basis of one-dimensional and 3-D CFD-based numerical simulations. Furthermore, some gas-handling design methods that have been used to increase the multiphase flow-handling ability of ESP are analyzed in Section 5, followed by the conclusions and future recommendations.

2. Flow Mechanism in Multi-Stage Centrifugal Pump

The ESPs are widely used in oil and gas industries because of their high versatility and efficiency. ESP is a multi-stage pump (see Figure 1) with impellers of backward-curved blades. The impellers are placed on a single shaft powered through an induction motor. The water enters into the impeller flow channel through the impeller eye and is thrown radially outward by the centrifugal motion. As a result, the liquid gains both pressure and kinetic energy. In order to pass this water to the subsequent impeller, a fixed device called a diffuser is applied to deflect the water and make it prepared for the subsequent impeller attached to the outlet of the diffuser. The sequence of impellers, coupled together, multiplies the pressure gained at each stage. That is why multi-stage pumps generate higher values from the pressure head [18]. The high-pressure head and flow rate characteristics make submersible pumps an ideal choice for bore well lifting, firefighting and oil well lifting. There is no narrow flow region in the impeller and diffuser section of the submersible pump, which also makes it an ideal choice for wastewater pumping and lifting highly viscous fluids.
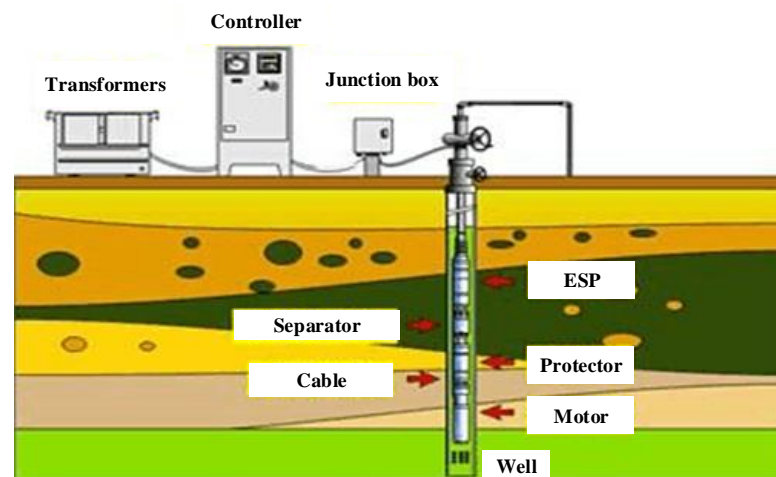
Figure 1. Electrical submersible pump (ESP) assembly and components.

2.1. Types of ESP Based on Stage Geometry and Specific Speed

The ESPs are mainly multi-stage centrifugal pumps with several stages assembled together in a casing. A casing may consist of 8–300 stages depending on their application. The ESPs could be categorized into three types: mixed, radial, and axial, on the basis of stage geometry. ESPs with radial geometry (see Figure 2a) are generally used for the production of the larger head and have a capability of handling inlet gas volume fractions (GVFs) < 10% [19], while the mixed-flow designs (see Figure 2b) are used for the production of higher flow rates and can handle the inlet GVFs up to 40% [20]. Mixed-flow designs are considered to be the best choice for handling two-phase flow conditions. On the other hand, axial flow designs (see Figure 2c) with helical impeller blades and axial diffusers are capable of handling high GVFs up to 90% [21,22] but exhibit smaller head compared to mixed and radial flow geometries.

(**a**) (**b**) (**c**)
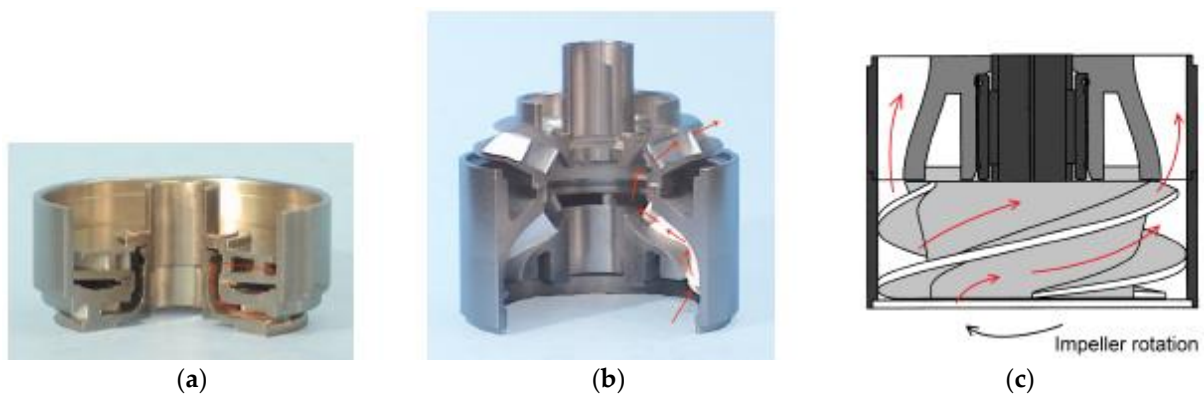
Figure 2. Representation of radial, mixed and axial flow geometries with impeller and stationery diffuser. The red arrows indicate the flow path [23]. (**a**) Radial geometry; (**b**) mixed geometry; (**c**) axial geometry.

ESPs can also be classified by the pump specific speed N_s. This non-dimensional parameter (N_s) can be determined by calculating the pump flow rate and head at BEP (best efficiency point).

$$N_s = \frac{\omega \left(Q_{BEP}\right)^{1/2}}{\left(H_{BEP}\right)^{0.75}}$$

(1)

where Q_{BEP} = design rate (gpm); H_{BEP} = design head (ft); ω = rotating speed (rpm).

From Equation (1), the pumps with a specific speed N_s < 1500 are normally considered as radial pumps and exhibit high head and low flow rate, while the pumps with specific speed N_s > 8000 are usually considered in the axial pumps category, showing a low head

and high flow rate. On the other side, mixed-flow pumps usually fall in between radial and axial pumps and have a specific speed between $1500 < N_s < 8000$. This dimensionless number is extremely used in industries for comparing various pump geometries.

In addition, the ESPs can also be described on the basis of pump curves, which contain brake horsepower, head and efficiency, in terms of flow rate and rotational speed, proposed by Pessoa and Prado [9]. They have developed pump performance curves on the basis of the manufacturer's catalog for the GC6100 ESP model, which is running at 3500 rpm rotational speed. Figure 3 is an example representation, extracted from the pump performance curves provided by Pessoa and Prado [9], which was determined by experiments with water as a working fluid.
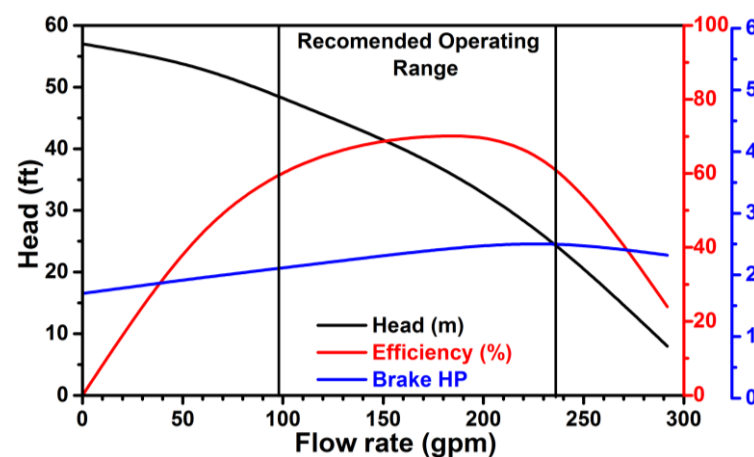

Figure 3. Hydraulic pump performance curve with water as working fluid [9].

From Figure 3, the BHP (brake horsepower) curve is used to size the motor, and the declining head curve is useful in sizing the pump. For a multi-stage ESP, the sizing is quite simple for water wells. However, designing an ESP with water data, for oil wells handling gas–liquid two-phase flow conditions, is difficult because of the mixture density at each stage. In this paper, the major aim is to analyze different research methods to increase the gas-handling ability of ESP models under two-phase flow.

2.2. Flow Velocity Triangles

The flow velocity triangles are used to represent the internal flow behavior of the fluid within the pump impeller. These triangles are constructed on the basis of the Euler pump equation [24], which is a powerful concept for designing an ESP system. The Euler equation is described in terms of the total pressure assuming no frictional losses (Equation (2)) [23,25].

$$\Delta p_T = \rho \omega (R_2 V_{u2} - R_1 V_{u1}) \tag{2}$$

where ρ = density of the fluid; ω = rotational speed; R_1 and R_2 = radii at impeller inlet and outlet, respectively; V_{u1} and V_{u2} = absolute component of tangential velocity at inlet and outlet, respectively.

Figure 4 is the representation of velocity triangles at the inlet and outlet of an ESP, described using three velocity components; tangential velocity (U), absolute velocity ($V = U + w$) and the relative velocity (w). From Figure 4, w_u and V_u are the relative and absolute component of tangential velocity, respectively. These components assist in calculating the meridional component of absolute velocity ($w_m = V_m = Q\sin\alpha/2\pi Rh$), which is defined as a function flow rate (Q) at a constant height (h). Finally, it helps in determining the absolute component of tangential velocity ($V_u = V - V_m$) used in the Euler pump equation.
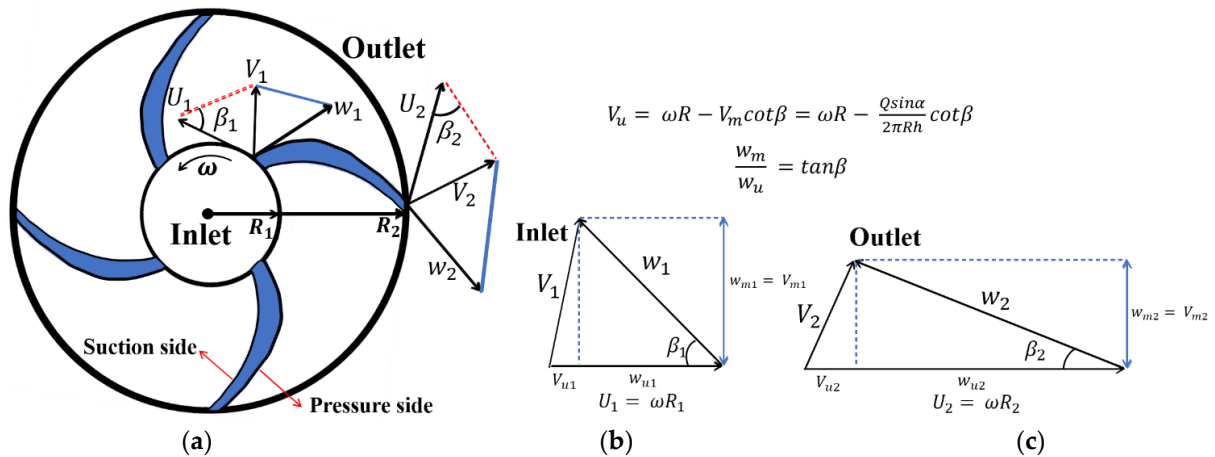
$$V_u = \omega R - V_m cot\beta = \omega R - \frac{Qsin\alpha}{2\pi Rh}cot\beta$$

$$\frac{w_m}{w_u} = tan\beta$$

Figure 4. Flow mechanism representation by velocity triangle. (**a**) Flow velocity diagram of the impeller having four blades; (**b**) velocity triangle at an inlet; (**c**) velocity triangle at an outlet.

Furthermore, by evaluating the velocity triangles in relation with the flow components at inlet and outlet, Equation (2) for total pressure rise becomes the following:

$$\Delta p_T = \rho\omega^2 \left(R_2^2 - R_1^2\right) + \rho\omega\frac{Qsin\alpha}{2\pi h}(cot\beta_1 - cot\beta_2) \tag{3}$$

As the flow has no pre-rotation when $V_{u1} = 0$, thus

$$\Delta p_T = \rho\omega^2 R_2^2 - \rho\omega\frac{Qsin\alpha}{2\pi h}(cot\beta_2) \tag{4}$$

Since α is 90°, and, regarding basic trigonometric rules, $cot\beta_2 = 1/tan\beta_2$. Therefore, the final equation of total pressure rise becomes

$$\Delta p_T = \rho\omega^2 R_2^2 - \rho\omega\frac{Q}{2\pi htan\beta_2} \tag{5}$$

Furthermore, the total pressure rise in the ESP system can be best explained in terms of its theoretical head [9,25], determined as

$$H_E = \frac{\Delta p_T}{\rho g} \tag{6}$$

Then, by comparing Equations (5) and (6), we can obtain the theoretical head for the ESP impeller, known as the Euler head, proposed by Jiang [26] and Si et al. [27–30].

$$H_E = \frac{\omega^2 R_2^2}{g} - \frac{Q\omega}{2\pi ghtan\beta_2} \tag{7}$$

where ω = rotational speed of the impeller; β_2 = blade outlet angle.

In addition, the performance curves for any kind of pump can be fully understood by introducing four simple relations: theoretical head coefficient ($\psi_{tp,th}$), head coefficient (ψ_{tp}), flow coefficient (φ), and hydraulic efficiency (η). The following relations are derived specifically for ESPs in relation to Equation (7) [23,31].

$$\psi_{tp} = \frac{gH}{\omega^2 R_2^2} \tag{8}$$

$$\psi_{tp,th} = \frac{\psi_{tp}}{\eta} \tag{9}$$

$$\varphi = \frac{Q}{\omega R^3} \tag{10}$$

$$\eta = \frac{Q \Delta p}{\tau \omega} \tag{11}$$

where τ = torque needed to drive the motor shaft; $\psi_{tp,th}$ = two-phase flow theoretical head.

An example regarding the well application of these relations for determining the centrifugal pump performance handling two-phase flow is shown in Figure 5a–c, conducted by Si et al. [27–29]. An obvious degradation in the pump head and efficiency can be observed by the influence of increasing gas volume contents (see Figure 5a,b). However, an abrupt decrease in pump performance happens when IAVF (inlet air volume fraction) is more than 8% for all flow rates. On the contrary, the theoretical head coefficient curve (see Figure 5c) has justified the concept of obvious losses, which was the same regardless of IAVF values (up to 8%). Due to this reason, several researchers have started defining the head ratio ($\psi^* = actual\ head\ cofficint/\psi_0$) while performing the two-phase flow performance modifications.
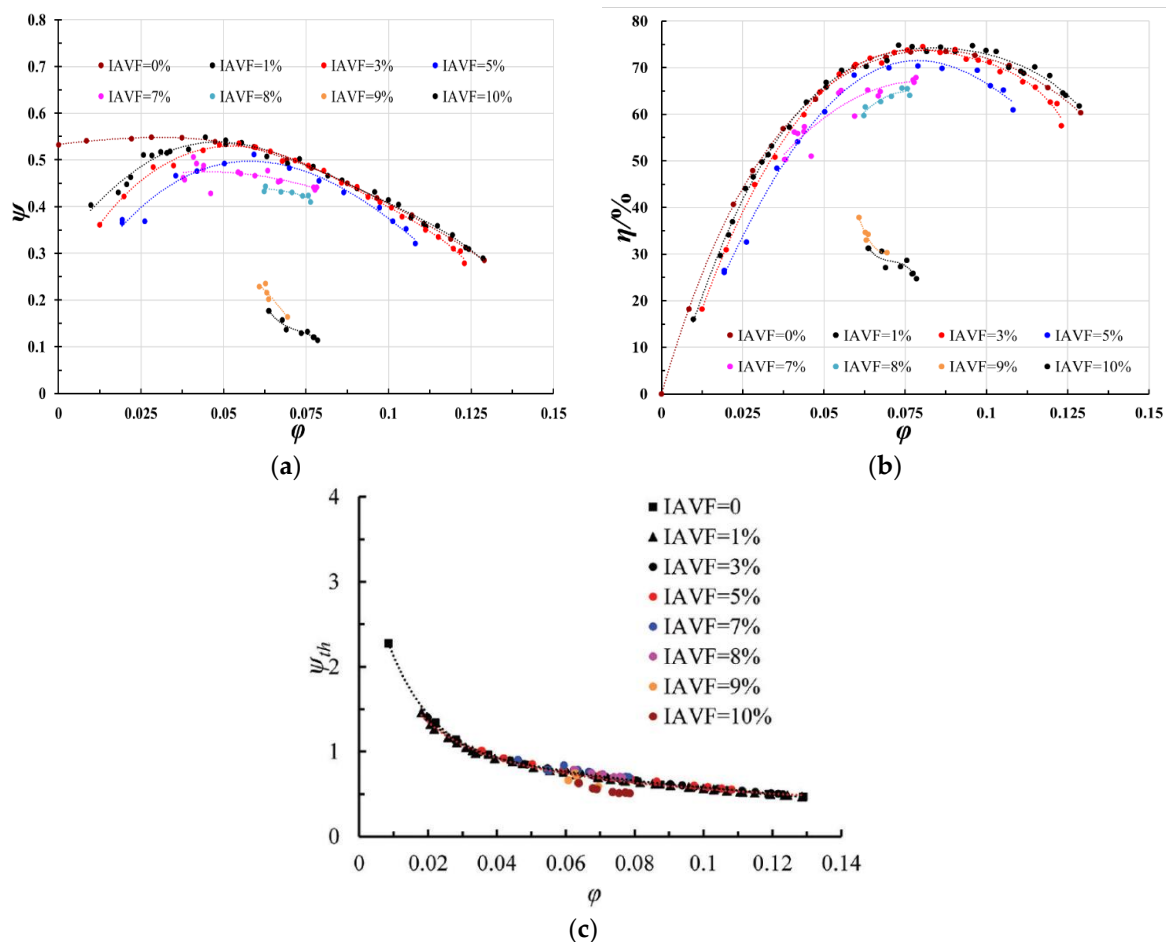
Figure 5. Pump performance curves at 2910 rpm rotational speed [27–29]. (**a**) Flow coefficient against head coefficient, (**b**) flow coefficient against efficiency, (**c**) theoretical head curve.

The aforementioned relations have always played an important role in explaining the pump performance curves as well as the flow behavior inside the pumps in a simple way. However, the actual flow behavior of the fluid within the multi-stage pump impeller is much more difficult to understand when handling two-phase flow because of its complex geometry. Therefore, the following sections report some recent experimental and numerical

investigations on the internal flow behavior and the gas-handling capability of multi-stage centrifugal pumps.

3. Experimental Analysis

The experimental studies have an advantage of predicting the basic parameters that influence the pump behavior when handling gas–liquid two-phase flow. These parameters are rotational speed, GVFs of mixed flow, bubble-size, liquid flow rate and fluid viscosity. Experimental analysis of ESPs handling two-phase flow basically includes the empirical approaches, flow visualization, GVF, bubble size measurement and viscosity analysis.

3.1. Empirical Approach

The two-phase flow experiments regarding the empirical approach are based on four basic concepts: pump head, free-gas fraction, surging initiation and gas-lock condition. A summary of the experimental studies on ESP gas-handling performance based on empirical approach is listed in Table 1.

Table 1. Experimental analysis on ESP gas-handling performance based on empirical approaches.

Reference	Analysis	Pump Model Type and Fluid
Lea (1982) [32]	Multi-phase flow performance of 3 distinct ESPs handling gaseous fluids	Two radial pumps, I-42B and C-72, and K-70, a mixed-flow pump; water–air and diesel–CO_2, two-phase mixture
Turpin (1986) [33]	Development of empirical correlation for predicting centrifugal pump's performance working under two-phase flow conditions	Same as Lea [32]
Cirilo (1998) [34]	Two-phase flow performance comparison among three different submersible pumps	Two mixed-flow pumps and one radial flow design; water–air
Pessoa (1999) [35]	Investigates gas-handling capability of tapered pump working with light/heavy oil and gas	Axial-flow pump with mixed-flow geometry; crude-oil/gas
Romero (1999) [36]	Two-phase flow performance evaluation of an ESP working with gas-handling device with slotted rotor	Mixed-flow pump with slotted impeller; water–air
Sachdeva (1988) [37]	Evaluates the working capability of ESPs (used in petroleum industry) under two-phase flow conditions	Same as Lea [32]
Sachdeva (1992) [38]	Correlates two-phase performance of ESPs working under gaseous conditions	Same as Lea [32]
Duran (2003) [39]	Correlation development for ESP two-phase performance prediction	Commercial ESP (series 513 having 6100 B/D at BEP); air–water
Zhou (2010) [12]	Improves and modifies Sachdeva's correlation for gas–liquid performance prediction of ESPs in gassy well	Same as Lea [32] and Sachdeva [37,38]
Salehi (2012) [40]	Analyzes two-phase performance of the ESP using modelling of surging mechanism	ESP (TE2700); water–air
Mohammadzaheri (2015, 2019) [41,42]	Introduces artificial neural network (ANN) for two-phase head predication in ESPs, as a substitute of existing empirical models	Radial (I-42B) ESP used in Lea's [32] experiments; two-phase petroleum fluids
Zhu (2017–18) [26,43]	Investigates the liquid–gas two-phase flow behavior in ESP by conducting experiments and modelling	Commercial ESP; liquid–gas
Zhu (2019) [44]	Development of a new mechanistic model to examine the gas–liquid flow patterns in ESP	ESP with capacity of 5000 B/D; air–water
Mohammadzaheri (2020) [45]	Proposes a shallow ANN model for the prediction of two-phase head and pressure increase in ESPs, as a replacement of existing empirical models	Radial (I-42B) ESP used in Lea's [32] test; two-phase petroleum fluids

From Table 1, one can see that the pioneering empirical approach in oil industry regarding the influence of free gas on the pump performance is conducted by Lea [32], in which three different ESP systems were examined using diesel–CO_2 and air–water as two-phase mixtures. The experiments were based on varying inlet GVFs (diesel/CO_2 = up to 50% and water/air = up to 11%) and intake pressures (diesel/CO_2 = 50–400 psig and water/air = 25–30 psig). The following conclusions were made by this study.

■   The influence of free gas on pump performance is more dangerous at lower intake pressures and lower inlet GVFs. However, it decreases with the increase in intake pressure.

■   Mixed-flow pumps are better than the radial flow pumps while handling gas–liquid two-phase flow.

■   The pumps perform better with diesel–CO_2 mixtures than the air–water mixtures.

Then, by using the same parameters as Lea [32], the pump intake pressure and GVF, Cirilo [34] also conducted some experiments to analyze the effect of air–water two-phase flow conditions on the performance of three different ESPs: two mixed-flow pumps with a design flow rate of 4000 B/D and 7000 B/D, and one radial pump with a design flow rate of 2100 B/D. The experiment results showed that the gas-handling ability of all three pumps is increased with the increase in intake pressure. Furthermore, the mixed-flow pumps were capable of handling gas greater than 30% GVF and showed less degradation compared to the radial flow pump which handled < 10% GVF and showed the highest degradation. Additionally, he took the mixed-flow pump with design flow rate 4000 B/D (26.5 m^3/h) under consideration and examined the influence of the number of stages on the gas-handling performance of ESP as shown in Figure 6. Figure 6 is drawn on the basis of Cirilo's [34] data, which show that the head degradation decreases as the number of stages increases. The pump with the minimum number of stages shows the highest decline in the head curve.
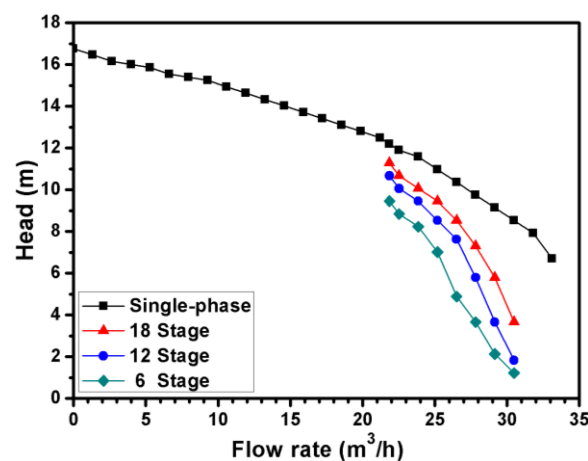

Figure 6. Performance curve for a mixed-flow pump with a different number of stages with best efficiency point (BEP) = 26.5 m^3/h (4000 B/D) and free gas = 15% [34].

Then, based on Lea's [32] experimental data for ESPs, researchers, such as Turpin [33], Sachdeva [38], Zhou [12], have established some empirical correlations for predicting the performance of pumps working under gassy conditions, while Romero [36] has developed an empirical correlation on the basis of Cirilo's [34] experimental data. Then, later, Duran [39] also established a correlation in order to extend the application circle of Turpin [33] and Romero [36]. A detailed information about these correlations, their related parameters and application range are provided in Table 2 as a function of H_m and Δp_m, where H_m is the head of the gas–liquid mixture and Δp_m is the pressure rise in gas–liquid mixture.

Table 2. Empirical correlations used for pump performance prediction at multi-phase flow conditions.

Reference	Empirical Correlation	Related Parameters	Application Range
Turpin (1986) [33]	$H_m = He^{-a_1(q_G/q_L)}$ $a_1 = \left(\frac{346430}{(0.145p_{in})^2} \right) \frac{q_G}{q_L} - \frac{410}{0.145p_{in}}$	H = single-phase head (m) p_{in} = intake pressure (kpa) q_G, q_L = flow rates of gas and liquid at inlet (m^3/d)	Pump performance prediction
Sachdeva (1992) [38]	$\Delta p_m = \left(\frac{K}{0.145} \right)(0.145p_{in})^{E1}(\alpha)^{E2}(0.1835q_L)^{E3}$	Δp_m = pressure increment (kpa/stage) α = free gas content (stage intake)	Pressure rise in ESP and pump performance prediction
Romero (1999) [36]	$H_{dl} = \left(1 - \frac{q_{dl}}{q_{dmax}} \right)\left\{ a\left(\frac{q_{dl}}{q_{dmax}} \right)^2 + \frac{q_{dl}}{q_{dmax}} + 1 \right\}$ $a = 2.902\lambda_G + 0.2751$ $q_{d\,max} = 1 - 2.0235\lambda_G$ $\lambda_G = 0.004(C_1 p_{in})^{0.6801}$	q_{dl} = dimensionless liquid flow rate (q_L/q_{max} (manufacturer's catalog curve)) $H_{dl} = \frac{H_m}{H_{max}}$ = dimensionless two-phase head	Less degradation in ESP performance or dispersed bubbly flow
Duran (2003) [39]	Bubbly flow, $\Delta p_m = (1-\alpha)\rho_l H\left(\frac{q_l}{1-\alpha} \right) + \alpha\rho_g H\left(\frac{q_g}{\alpha} \right)$ Elongated bubbly flow, $\Delta p_m = (a + b\ln(q_{Gn}))/C_1$ $q_{Gn} = (1-\alpha)\left(\frac{q_G}{q_{max}} \right)$	α = in-situ GVFs q_{Gn} = normalized gas flow rate $a = -0.47075$ $b = -0.21626$	Slight and severe head degradation
Zhou (2010) [12]	$H_{dl} = K(0.145p_{in})^{\alpha E1}(1-\alpha)^{E2}\left(1 - \frac{q_m}{q_{max}} \right)^{E3}$ $q_m = \frac{q_L}{(1-\alpha)}$	$H_{dl} = \frac{H_m}{H_{max}}$ = dimensionless two-phase head	Low and high head degradation or bubbly flow and churn flow
Mohammadzaheri (2015, 2019) [41,42]	ANN fully connected cascade (FCC) model, $H_m = \sum\limits_{i=1}^{5} T_i f(W_{i1}p_{in} + W_{i2}q_m + W_{i3}\alpha + B_i) +$ $(C_1 p_{in} + C_2 q_m + C_3\alpha) + b$	W and T = first and second-layer weights; C = matrix of cascade connection weights; B_i and b = biases	Pressure rise and head prediction, two-phase flow in ESP
Mohammadzaheri (2020) [45]	Shallow ANN model, $H_m = \sum\limits_{j=1}^{3} T_j f\left(\sum\limits_{i=1}^{3} W_{ij}u_i + b_j \right) + b$	p_{in}, q_m and α, represented as ui, i = 1–3; W_{ij} and Tj = first and second-layer weights; bj and b = biases	Pressure rise and head prediction, two-phase flow in ESP

According to Table 2, all the previous correlations developed by Turpin [33], Sachdeva [38], Romero [36], Duran [39], and Zhou [12] have been applied for the prediction of multi-phase performance of the ESPs in terms of head degradation and free-gas content. Among these, Zhou's correlation [12] was established in order to improve and modify the Sachdeva's correlation [38]. They used dimensionless head for two-phase flow analysis instead of pressure rise, and their empirical model was able to predict the pump performance when the transition happens between the bubbly flow and gas pockets (surging) with the change in inlet gas content. Additionally, the values of coefficients (K, Kc, E1, E2, E3, E4, and E5), used in Sachdeva [38] and Zhou's correlations [12], are given in Table 3. Furthermore, the correlations proposed by Mohammadzaheri [41,42,45] were developed using different ANN, as a replacement to existing empirical models. Their ANN models have shown better prediction of the two-phase performance compared to existing models.

Table 3. The values of correlation coefficients for mixed-flow pump K-70.

Study	Pump Type	K	Kc	E1	E2	E3	E4	E5
Sachdeva (1992) [38]	Mixed (K-70)	0.0936583	_	0.622180	−1.350338	−0.31704	_	_
	Radial (I-42B)	1.154562	_	0.943308	−1.175596	−1.30009	_	_
	Radial (C-72)	0.1531026	_	0.875192	−1.764939	−0.91870	_	_
Zhou (2010) [12]	Mixed (K-70)	1.236426	7.497750	2.570713	12.66051	0.75505	−0.34870	0.86709
	Radial (I-42B)	1.971988	1.418884	1.987836	9.659564	0.90591	−0.07244	0.31854
	Radial (C-72)	1.401067	2.173723	3.100355	14.93852	1.30836	−0.05253	0.83359

3.1.1. Comparison of Different Correlation Models

In order to analyze the validity and accuracy of previous correlation models, the pump performance test analysis performed by our research team [46] is used for comparison among different empirical models (Table 2). The data sets shown in Table 4 are taken from a single-stage radial flow centrifugal pump at two different rotational speeds (1000 rpm and 1450 rpm) and gas void ratios (GVRs). This also concerns the effect of different rotational speeds on different correlation models used for performance prediction of pumps having half open impellers with volute. The mixture flow rate is calculated by the sum of gas and liquid flow rates while the pressure increase is measured by the change in pressure between inlet and outlet. The instability in pumping operation (surging) started when the mixture rate is less than 301.88 m^3/d (1000 rpm) and 366.32 m^3/d (1450 rpm) conditions.

Table 4. Test data of single-stage radial flow pump at two different rotational speeds and gas void ratios (GVRs).

Rotational Speed	Gas Void Ratio (%)	Mixture Rate (m^3/d)	Pump Intake Pressure (kpa)	Mixture Density (kg/m^3)	Pressure Increase (kpa)
1000 rpm	4.2	338.2	132.70	957.20	22.70
	4.2	343.22	132.65	957.20	22.49
	4.2	328.18	133.00	957.20	22.28
	4.2	313.15	133.44	957.20	22.58
	4.2	303.13	133.62	957.20	22.73
	4.2	301.88	133.71	957.20	22.44
1450 rpm	5	562.86	125.90	949.21	41.01
	5	510.32	127.39	949.21	45.12
	5	482.53	128.96	949.21	46.15
	5	442.11	130.15	949.21	47.89
	5	386.53	132.05	949.21	51.84
	5	366.32	133.61	949.21	49.76

As shown in Figure 7a,b, the dimensionless head (H_{dl}) for actual data sets is calculated through Equation (11) (ratio between the mixture and maximum head), while the mixture head is calculated by Equation (12), using the pressure increase values from

Table 4. Moreover, the mixture density is calculated through Equation (13). In addition, dimensionless liquid rates for actual data sets are calculated through the equation provided in Table 3 (ratio between in-situ liquid rate and maximum liquid rate).

$$H_{dl} = H_m / H_{max} \tag{12}$$

$$H_m = C_3 \Delta p_m / \rho_m \tag{13}$$

$$\rho_m = \rho_G \lambda_G + \rho_L (1 - \lambda_G) \tag{14}$$

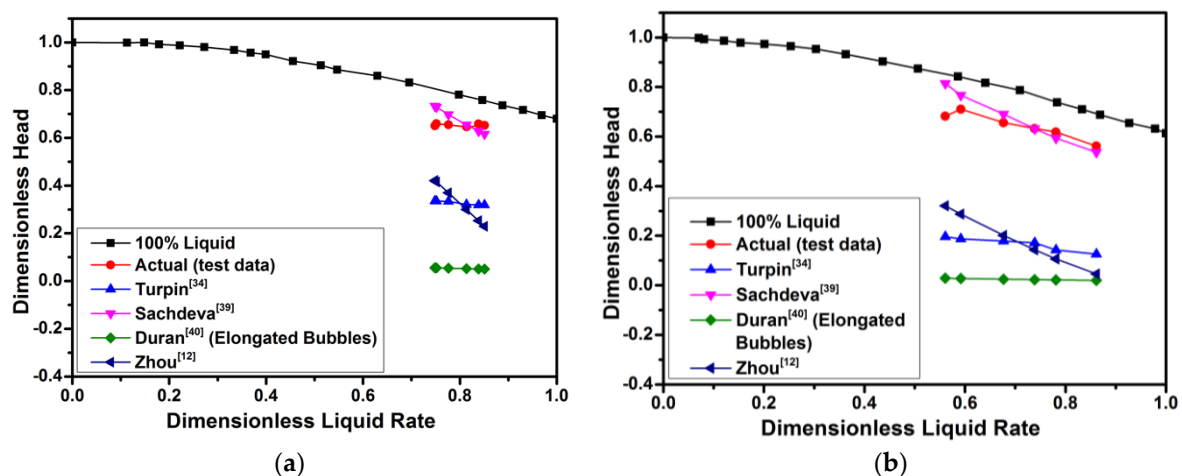where C_3 = conversion unit factor (101.945).

Figure 7. Comparison of different empirical models using our test analysis; (**a**) 1000 rpm, (**b**) 1450 rpm.

The dimensionless heads for the rest of the empirical models are calculated through their respective correlations from Table 3. In addition, the previous analysis on the radial flow pump performed by Zhou [12] highlighted that the accuracy of the correlation model is strongly dependent on the pump BEP. According to Zhou [12], if the BEP is greater than 352 m^3/d, coefficients (K, E1, E2, and E3) for C-72 pump should be used for calculation (Table 3). For smaller radial pumps (<352 m^3/d), coefficients for I-42B pump are suitable to use for calculations. Therefore, the dimensionless head for Zhou's [12] data is calculated using coefficients for C-72 radial pump. The Romero's [36] model cannot be applied for the test data in Table 4 because his correlation was built specifically for the mixed-flow pump.

The empirical correlation proposed by Duran and Prado [39] for the bubbly flow model does not produce any answers for both analyses (1000 rpm and 1450 rpm) in Table 4. This is because the calculated values of $q_L/(1 - \alpha)$ surpasses the maximum values of flow rate, and thus it is not possible to obtain the value of the head from the pump curve through $H[q_L/(1 - \alpha)]$ (see Duran's [39] equation in Table 4). On the contrary, the correlations of Duran and Prado [39] for elongated bubbles yield positive but lower values of pressure increase (Δp_m) for both data sets in Table 4. Additionally, their dimensionless values of the head are very poor compared to other empirical models (see Figure 7a,b). In order to get higher values of pressure increase close to actual data, the normalized gas flow rate needs to be very low around 3.574×10^{-8} (1000 rpm) and 4.31×10^{-13} (1450 rpm), which is impossible to achieve with the given values of GVR, because the maximum normalized gas flow rate in our case is 0.03574 and 0.0431, respectively. This indicates that both correlations established by Duran and Prado [39] are not applicable to the data set in Table 4, which makes them more specific to the type of pump evaluated.

From Figure 7a,b, one can see that both analyses (1000 rpm and 1450 rpm) have shown similar trends for all different models and Sachdeva's [38] curve is in best agreement with both data sets in Table 4. Meanwhile, Turpin's [33] model is the second and Zhou's [12] model is the third. Both Duran et al. [39] and Romero's [36] model could not provide good

results for the actual data set in Table 4, even their correlations were established on the basis of the air–water mixture.

The reason why most of the empirical models produce poor performance is because their models were established for high inlet pressure (for example, in the case of Turpin, 344.73 kpa, 689.47 kpa and 1378.95 kpa), no water, but oil and CO_2, multistage arrangement, different rotational speed (compared with our experimental results) and different pump geometries. Consequently, these empirical models become more specific and valid for the pump categories evaluated. This is the reason why we have tried to compare our simpler centrifugal pump models, in order to determine the validity and operating range of these empirical models.

3.1.2. Comparison of Different Surging Correlations

Since the pump performance becomes worst at higher inlet gas contents because of the formation of gas pockets (Surging) [47], the pump encounters severe instability and vibration. Therefore, Turpin [33], Cirilo [34], Romero [36], Duran [39], Gamboa [47], and Zhu [43,44] have further developed some correlations dealing with pump instability or surging on the basis of pump intake pressure, critical free-gas content and flow rates. The available surging correlations for analyzing the stability and instability in pumping operation are listed in Table 5.

Table 5. Empirical correlations used to predict pump instability or surging in two-phase flow conditions.

Study	Empirical Correlation	Related Parameters
Turpin (1986) [33]	$\phi_s = 2000\left(\frac{1}{3C_1 p_{in}}\right)\left(\frac{q_G}{q_L}\right)$	ϕ_s = Criterion to predict pump stability and instability
Cirilo (1998) [34]	$\lambda_G = 0.0187(C_1 p_{in})^{0.4342}$	λ_G = Critical gas volume content
Romero (1999) [36]	$\lambda_G = 0.004(C_1 p_{in})^{0.6801}$	$C_1 = 0.145$
Duran (2003) [39]	$\frac{q_G}{q_{max}} = \left(5.580\left(\frac{\rho_G}{\rho_L}\right) + 0.098\right)\left(\frac{q_L}{q_{max}}\right)^{1.421}$	$\frac{q_G}{q_{max}}$ and $\frac{q_L}{q_{max}}$ = normalized gas and liquid rate at surging point, respectively
Zhou (2010) [12]	$\left(\frac{q_L}{q_{max}}\right)_c = K_c(C_1 p_{in})^{E_4}(\alpha)^{E_5}(1-\alpha)$	
Gamboa (2011) [47]	$\frac{q_G}{q_{max}} = 0.102 exp\left(\frac{q_L}{q_{max}}\right)^{4.4682}\left(\frac{\rho_G}{\rho_L}\right)^{0.2}\left(\frac{\omega D^2}{v}\right)^{0.4}$	ω = pump rotational speed (rpm) v = fluid kinematic viscosity D = impeller outlet diameter (m)
Zhu (2017–19) [26,43,44]	$\lambda_G = \dfrac{2\left[\frac{0.4\sigma}{(\rho_L - \rho_G)\Omega^2 R_I}\right]^{0.5}}{10.056\left(\frac{\sigma}{\rho_L}\right)^{0.6}\left(\frac{\Delta p_m Q_L}{\rho_L V}\right)^{-0.4}\left(\frac{\rho_L}{\rho_G}\right)^{0.2}}$	σ = surface tension (N/m) Ω = angular speed (rad/s) Q_L = liquid flow rate (m^3/s) V = impeller volume (m^3) R_I = representative rotor radius (m)

From Table 4, Turpin's [33] correlation recommended a criterion (ϕ_s) to examine the stable and unstable operation of the pump working under multiphase flow conditions. The authors claimed that if the $\phi_s < 1$, the pump can work under gassy conditions in a stable way, and the actual head can be calculated using the head correlations. Furthermore, if the $\phi_s > 1$, the pump stability is disturbed by the presence of gas pockets (surging) which cause serious head degradation. However, referring to our data set in Table 4, the minimum calculated value of criterion ϕ_s is 1.507 (1000 rpm) and 1.811 (1450 rpm), which is greater than 1. Thus, the pump should be subjected to instability or surging according to Turpin's [33] assumptions, but the pump operation was stable for all the test analyses in Table 4. Therefore, Turpin's model could not be used to predict the surging mechanism.

For Cirilo's [34] surging model (from Table 5), the calculated critical value of GVR is 6.8% for both data sets in Table 4, which was taken at pump intake pressure 133.71 kpa (1000 rpm) and 133.61 kpa (1450 rpm). According to critical value of GVR from the model, stable pumping should be achieved by keeping the maximum GVR within 6.8%. Anyhow,

the pumping was stable until the gas void ratio (GVR) was less than 4.2% in the case of 1000 rpm analysis and 5% in the case of 1450 rpm analysis in Table 4, which is less than the maximum critical value of GVR predicted by the critical model. It means that Cirilo's [34] critical model provides satisfactory results for the given data set in Table 4. On the other hand, the calculated value of maximum GVR for Romero's [36] critical model (Table 5) is 3% for both data sets, which means the stable pumping should be achieved by controlling the maximum critical GVR's within 3%. However, the data in Table 4 were stable until the gas void ratio was less than 4.2% (1000 rpm) and 5% (1450 rpm). Thus, Romero's [36] critical model could not be applied to the data set in Table 4. This is possibly because the Romero's [36] model was built for a mixed-flow pump.

Then, for the critical model proposed by Duran and Prado [39], the calculated value of maximum critical normalized gas rate is 8.87% (1000 rpm) and 9% (1450 rpm), corresponding to the mixture flow rate values of 343.22 m^3/d and 562.86 m^3/d from test data in Table 4, respectively. Moreover, concerning all values of test data in Table 4, the maximum normalized gas flow rates for stable pumping operation were less than 3.4% (1000 rpm) and 4.3% (1450 rpm), which is less than the maximum critical value of normalized gas flow rate from the model but with a big difference between the actual and model predicted values. Thus, Duran and Prado's [39] critical model could be applied for the prediction of the surging mechanism in Table 4.

Furthermore, the dimensionless critical liquid rate, calculated by Zhou's [12] critical model (Table 5), is 0.399 (1000 rpm) and 0.419 (1450 rpm), which was taken at pump intake pressure of 133.71 kpa and 133.61 kpa (Table 4), respectively. However, the dimensionless liquid rate of the last stable points (301.88 m^3/d and 366.32 m^3/d) for the data sets in Table 4 are 0.748 and 0.561, respectively. Since the critical value from the model is lower than the last stable point for both data sets. Thus, Zhou's [12] critical model provides a good prediction of the data sets in Table 4.

In short, the surging critical models for Cirilo [34], Duran [39], and Zhou [12] offer a satisfactory simulation of both data sets in Table 4. The rest of the surging correlation models fails to predict the surging mechanism of the data sets. In addition, the rotational speed does not really have any effect on the empirical models for the prediction of both pump performance and surging mechanism. However, the actual pump performance analyses on our two data sets [46] (Table 4) have shown that the performance degradation of the pump running at lower rotational speeds (1000 rpm) was worse compared to higher rotational speeds (1450 rpm). Furthermore, our study has proved that the rotational speed is an important parameter that permits the pump to work better when handling multiphase flow conditions.

In addition, the previous studies and different trends in surging correlations show that the main reason behind surging initiation that causes the pump performance degradation is still unclear. The performance of any kind of pump handling two-phase flow is still difficult to predict accurately using empirical approaches because these correlations were established for multistage pumps. This means that most of the related works use at least five stages or more. The authors tried to establish performance correlations specific to these machines for which inlet pressure conditions are essential. Consequently, it was very difficult to use more physical parameters and most of the authors performed overall measurements to propose empirical laws that are, of course, only valid for the pump categories evaluated. This is the reason why others performed more specific research using much simpler arrangements such as centrifugal or mixed-flow single stages in order to get more local flow features. Moreover, the development of empirical models for an ESP is still challenging because of the complex geometry of its impeller and diffuser. Furthermore, for ESPs handling free-gas, it is also required to predict the factors (flow patterns, bubble size, surging initiation and gas-locking mechanism) accountable for head degradation [9]. Therefore, flow visualization techniques have been widely used in the past, in order to better understand these factors and their effect on ESP performance.

3.2. Flow Visualization and Bubble Size Measurement

Flow visualization techniques have primary importance in experimental studies of the ESP handling gas–liquid two-phase flow for examining the internal flow behavior, including bubble inception, bubble size and gas-pocket formation (surging). These techniques, in combination with the pump performance results, have an advantage in obtaining detailed information about flow pattern within the pump impeller. Therefore, several researchers have used the flow visualization techniques in the past to analyze the mixed-flow patterns inside the pumps. A high-speed camera is the basic experimental tool used for these techniques.

Murakami and Minemura [15,48] are considered to be the pioneers for introducing the first and basic experimental visual studies to investigate the influence of gas entrainment on hydraulic pump performance. By conducting experiments at different GVFs, they found out that the multiphase flow pattern is strongly influenced by the GVFs. At higher GVFs, the flow was unstable, causing vibrations inside the pump due to the formation of large gas pockets on the pressure side of the impeller blade. The author claimed that the presence of gas pockets is the main reason for the pump head degradation.

Since then, many researchers, such as Patel [49], Kim [50], Furukawa [51], Sato [52], Andras [53], Takemura [54], Estevam [10], Thum [55], Izturitz [56], Barrios [3,17], Schafer [57,58], Shao [59], Si [46], Cubas [60], have put their efforts towards flow visualization, in order to achieve complete information about bubble behavior within impeller and gas-pocket formation. Among these, Patel [49], Kim [50], and Takemura [54], Sato [52], and Thum [55] have discussed, in detail, the bubble agglomeration mechanism where Patel [49] and Kim [50] explained that the accumulation of the bubbles happens due to strong slippage effect between the liquid and gas phase which cannot be ignored inside the impeller flow channel. Meanwhile Takemura [54] proposed that the bubble agglomeration is closely related to high-pressure gradients and can be minimized by changing the blade load distribution. Furthermore, Sato [52] and Thum [55] suggested that the accumulation of bubbles and the formation of gas pockets are associated with the separated flow and are the main factors for pump head degradation. Both authors claimed that the formation of gas pockets happens on the pressure side of the blade. On the contrary, Andras [53] observed that gas-pocket formation occurs on the suction side of the impeller rather than the pressure side and seriously degrades the pump performance. Therefore, to minimize the effect of gas entrainment on pump performance, Furukawa [51] conducted a visual study on radial flow pump using a high-speed camera. They observed that the accumulation of gas occurs on the blade suction side, which leads the pump to form larger gas pockets and consequently deteriorate its performance. Their study also provided some empirical design considerations to reduce the bubble agglomeration.

- Impeller blade tip should be left open to reduce bubble accumulation by leakage.
- Impeller should have some recirculation holes in order to burst the bubbles.
- The use of higher outlet blade angle should be effective.
- Diffuser vanes have to be near the impeller outlet.

In addition, Shao et al. [59] and Si et al. [46] have performed visualization experiments in order to investigate different flow patterns accountable for pump performance degradation under two-phase flow conditions. Their experiments were conducted by changing IAVFs in order to analyze the gas-handling ability of the centrifugal pump, as well as to examine the effect of rotor-stator interaction on the pump performance deterioration. Shao et al. [59] have claimed that the flow inside the impeller flow channel remains as a bubbly flow structure when IAVF $\leq$ 3% and the bubble diameter increases with the increase in IAVFs, which was later justified by Si et al. [46]. Where they have further revealed that in volute region after the tongue, the bubbly flow regime can be observed at all values of IAVFs (see Figure 8a–f). An obvious alteration in the impeller flow channel can be observed from Figure 8a–f at higher IAVFs. This is because, with the increase in IAVFs, the smaller bubbles (uniform bubbles 0.5% IAVF) turn into larger air bubbles (agglomerated bubbles at 3% IAVF) and end up forming gas pockets (at 4% IAVF), which partially blocks the impeller flow passage and seriously causes pump performance degradation. A further increase in

IAVFs (at 4.2%) causes an abrupt change in flow structure near the tongue area where a strong gas separation can be observed close to the impeller outlet region, which blocks the entire impeller flow channel, though some isolated bubbles still exist. However, a further increase in IAVFs (>4.2%) will lead the pump to shut-off condition.
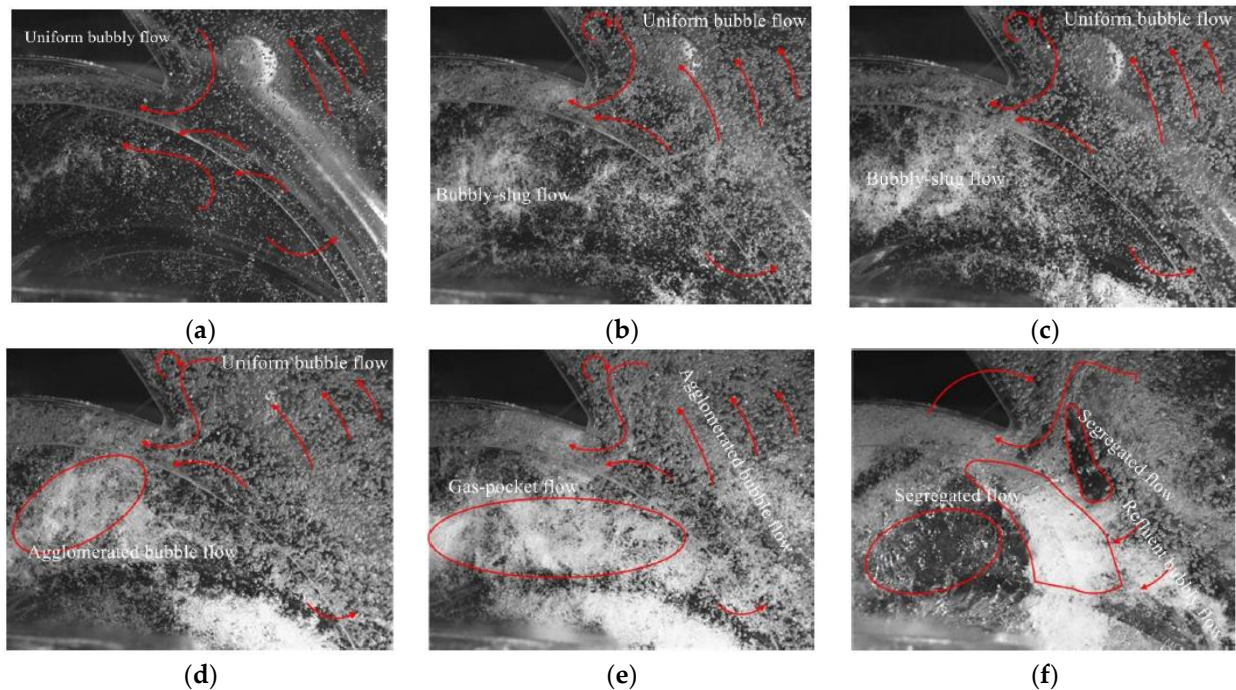

Figure 8. Different flow structures at $\varphi = 0.06$ for inlet air volume fraction (IAVF) [46]: (**a**) 0.5%; (**b**) 1%; (**c**) 2%; (**d**) 3%; (**e**) 4%; (**f**) 4.2%, shut-off condition.

Moreover, the gas accumulation, gas-pocket formation and surging initiation mechanism are strongly dependent on the bubble size and trajectories, proposed by Estevam [10], Izturitz [56], Barrios [3,17], Stel [61]. Thus, using high-speed imaging, Estevam [10] studied different flow regimes inside an ESP impeller and observed that the bubble size and the effect of forces acting on it are the major reasons for surging initiation. Their study provides an insight into how the bubble size changed with the increase in gas volume contents reaching up to 2–3 mm (critical bubble size). The author declared this critical size as a point of surging initiation, which was later confirmed by Barrios [3], and Barrios and Prado [17], where they studied the effect of changing GVFs and rotational speed on the multiphase handling ability of the ESP system using visualization techniques. The authors were able to predict the possible factors accountable for surging initiation and found out that the critical bubble size has a major role in surging inception and pump performance degradation. Moreover, the authors have also examined the effect of increasing rotational speed on the bubble size and found out that the increase in rotational speed has a positive effect on the pump performance. As the bubble diameter decreased at a high rotational speed, the impeller flow channel achieved higher stability. This fact was later justified by several authors such as Gamboa [11], Zhang [62], Verde [63] and Cubas [60].

Most recently, Cubas [60] investigated the multiphase flow-handling ability of the centrifugal pump using high-speed flow visualization. The authors presented four different flow patterns by changing the inlet GVFs, rotational speed and liquid flow rates, as shown in Figure 9a–d. The first three flow structures: bubbly flow, agglomerated bubbly flow and gas pocket, were already introduced by Trevisan [64] and Verde [63], while the fourth flow pattern named "Annular flow", which is produced at a lower liquid flow rate was proposed by Cubas' [60] study. At high flow rates and low GVFs, the bubbles inside the impeller flow channel are smaller in diameter and the movement of gas is the same as the dispersed

bubbles through the homogenous liquid phase, as shown in Figure 9a. The bubbles follow the same path as impeller geometry and flow, along with the liquid phase. However, some bubbles may deflect towards the pressure side of the blade near the impeller outlet. Under this flow pattern, the pump performance is nearly equal to the single-phase performance.
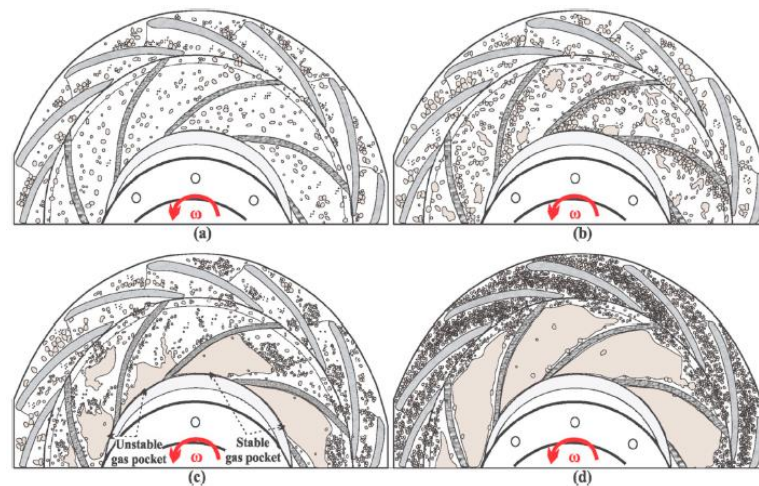

Figure 9. Gas–liquid flow structures in impeller and diffuser flow channels [60]. (**a**) Bubbly flow; (**b**) agglomerated bubbly flow; (**c**) gas pockets; (**d**) annular flow.

With the increase in inlet gas volume fraction, the dispersed bubbles start to agglomerate together to form bigger bubbles compared to bubbly flow. At this condition, the flow in both the impeller and diffuser is no longer homogenous, especially on the suction side of the blade, forming irregular-shaped gas pockets that are small in size. These small gas pockets are associated with the agglomerated bubbly flow as shown in Figure 9b. Moreover, under this flow regime, the impeller flow channel is subjected to severe liquid-phase turbulence and recirculation of bubbles, which affect the pump performance.

With a further increase in GVF, the dispersed and agglomerated bubbles are prone to strong collision and coalescence, forming a larger gas pocket that is associated with the surging initiation. Based on the observation (see Figure 9c), the air pockets were concentrated only on the suction side of impeller flow channels, while the diffuser channels were exposed only to bubble agglomeration. Additionally, these gas pockets produced can be stable/unstable in the system based on the intensity of the liquid-phase turbulence and wake generation behind the air pocket, which results in higher degradation in pump performance.

Furthermore, the annular flow, as shown in Figure 9d, is produced at very low liquid flow rates and very high GVFs and can severely deteriorate pump performance. This flow regime is mainly associated with the gas locking mechanism because the gas pockets become more stable and occupy the whole impeller flow channel in the form of elongated bubbles, which in turn cause pump operational failure. Notably, the diffuser flow channels are only prone to the intense agglomeration of bubbles and no gas pocket was observed in this section.

In contrast with all the previous visualization studies, Schafer et al. [57] have conducted a different type of approach for high-speed imaging, where they used Gamma-Ray tomography in order to investigate the gas-handling capability of centrifugal pumps. They observed that the inlet gas volume content (λ) was always lower than the average value of gas volume content (α_1) and the gas agglomeration happens near the inlet flow region of the pump. In addition, they drilled a recirculation hole in the impeller, the same as Furukawa [51], and found out that the accumulation of gas bubbles is less close to the drilled hole—as shown in Figure 10a,b. The abrupt change in gas distribution is observed near the inlet section when the value of λ varied between 1% and 3%. This abrupt alteration in the flow structure is due to the transition of bubbly flow into gas pockets. In addition,

this high-speed imaging has proved to provide a better imaging resolution compared to previous visualization techniques.
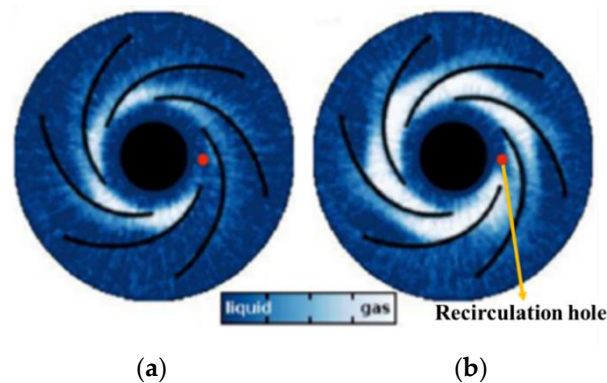

(**a**)   (**b**)

Figure 10. Unequal distribution of gas in the impeller running at 1480 rpm, produced by the recirculation hole [57], (**a**) λ = 1% and (**b**) λ = 2.6%.

3.3. Viscosity Analysis

Most of the previous experimental studies on ESPs have used water and air as a working fluid, but in oil and gas industries, ESPs have to deal with fluids with different viscosity. Thus, many researchers have conducted experiments in the past, in order to study the effect of viscosity on the performance of ESPs handling single-phase, as well as two-phase, flow. The summarized list of relevant studies is represented in Table 6.

Table 6. Test studies on ESPs handling viscous fluids under single-phase and two-phase flow.

Study	Analysis	Experimental Methodology and Observation
Ippen (1946) [65]	Single-phase flow	More than 200 experiments were performed at different rotational speeds and for oil viscosities around 10,000 SSU (303.03 centistokes) to predict the viscosity effects on pump performance
Hydraulic institute (1948) [66]	Single-phase flow	Based on water data, correction factors were developed for centrifugal pump performance working under viscous fluids conditions
Stepanoff (1957) [67]	Single-phase flow	Developed correction factors similar to the Hydraulic institute [66] in addition to Reynolds correlation
Gülich (1999) [68,69]	Single-phase flow	Analyzed the accuracy of correlations developed by the Hydraulic institute [66]
Añez (2001) [70]	Two-phase flow	Influence of free-gas entrainment and fluid viscosity on working capability of an ESP using gas, water and oil (375 Cp)
Turzo (2001) [71]	Single-phase flow	Developed equations on the basis of the Hydraulic institute [66] data, in order to examine the pump performance
Amaral (2009) [72]	Single-phase flow	Evaluate the correlations and charts developed by the Hydraulic institute [66]
Solano (2009) [73]	Single-phase flow	Similar observation as Amaral [72]
Trevisan (2009) [64]	Two-phase flow	Flow pattern analysis on ESP handling viscous fluids under two-phase flow condition
Trevisan and Prado (2010) [74]	Two-phase flow	Flow pattern analysis on ESP handling viscous fluids under two-phase flow condition
Bannwart (2013) [75]	Two-phase flow	Analyzed the effect of free-gas fraction and different liquid viscosities on the pump performance
Banjar (2013) [7]	Two-phase flow	Similar experiments as Trevisan [64,74] were observed
Paternost (2015) [76]	Two-phase flow	Free-gas entrainment effect on pump performance with an increase in liquid viscosity

Table 6. *Cont.*

Study	Analysis	Experimental Methodology and Observation
Zhu (2016) [77]	Single-phase flow	Effect of oil with different viscosities on the pump performance at different flow rates and rotational speeds
Zhang (2017) [78]	Single-phase flow	Examined the pump performance parameters with the increase in fluid viscosity; pipe viscometer was used to measure viscosity
Valdes (2020) [79]	Single-phase flow	Pioneer study to investigate the influence of Newtonian and non-Newtonian viscous fluids on ESP performance

Ippen [65] has conducted the first experimental research regarding the viscosity effect on multiphase pump performance. Based on the aforementioned test methodology (Table 6), the author has developed three different ratios: the ratio between oil head and water head ($\frac{H_o}{H_w}$), the ratio between oil horsepower and water horsepower ($\frac{BHP_o}{s_o.BHP_w}$), and the ratio of loss in efficiency ($\frac{100-e}{100}$). The author has further developed the Reynolds number (R_N) for viscous fluids, which was determined as:

$$R_N = 2620 \frac{\omega D_2^2}{\nu.10^5} \tag{15}$$

where ω and D_2 = rotational speed (rpm) and diameter (ft) of the rotor, respectively; ν = kinematic viscosity measured in cSt.

Then, by plotting these relations against the Reynolds number (Equation (14)), the author observed that with the increase in viscosity, the head decreases while the efficiency losses and input horsepower become higher.

Furthermore, Stepanoff [67] and the Hydraulic institute [66] have developed similar correction factors for head and flow rate for pumps handling fluids with high viscosity. If the performance curve for water is known, these factors can be defined as:

$$C_Q = \frac{Q_{vis}}{Q_w} \tag{16}$$

$$C_H = \frac{H_{vis}}{H_w} \tag{17}$$

where C_Q and C_H = correction factors for flow rate and head, respectively, while Q_{vis}, Q_w and H_{vis}, H_w = respective values of flow rate and head for viscous/water fluid.

These correction factors can be correlated with each other by the following expression (Equation (14)) defined by Stepanoff [67], which is useful for accurately predicting the *H–Q* curve under viscous fluid if plotted against the Reynolds number (Equation (15)).

$$C_Q = (C_H)^{3/2} \tag{18}$$

$$R_{N(stepanoff)} = 6.0345 \frac{\omega Q_{vis}}{\sqrt{H_w}\,\nu} \tag{19}$$

Anyhow, the accuracy of expressions (Equations (12) and (13)) developed by the Hydraulic institute [66] was challenged by Gülich [68,69], because of their narrow application range of specific speed. Then, later, Amaral [72] and Solano [73] have further declared that the correlations and charts defined by the Hydraulic institute [66] are insufficient for the pump performance prediction under viscous oil flow, while Verde's observation regarding Hydraulic institute [66] charts concluded that the charts were better for head prediction instead of capacity and efficiency.

Moreover, Trevisan [64], Trevisan, and Prado [74] have conducted visualization experiments to examine the effect of viscous fluids on ESP performance working under multiphase flow conditions. They found out that the impeller flow channel was occupied by four different types of flow patterns: agglomerated bubbly flow, air pockets, segregated

bubbly flow, and intermittent bubbly flow. The authors claimed that, with the increase in viscosity, the gas pockets were produced in the impeller flow channel even at low intake GVFs and caused serious head degradation in the ESP. Similar considerations were proposed by Banjar [7].

In comparison with the previous test studies, most recently, Valdes et al. [79] have conducted the first experimental study focusing on the comparative effect of viscous Newtonian and shear thinning non-Newtonian fluids on the ESP's performance. It was evident from their study that the frictional losses associated with fluid viscosity have proved to be major contributors to the ESP's performance degradation. The authors concluded that the performance of ESPs handling shear thinning nature fluids has improved significantly. The increase in the average head was about 23.5% while average efficiency was increased up to 15%. This concluding statement stands right even at larger values of effective viscosities for non-Newtonian fluids. This study provides an insight that the Shear thinning non-Newtonian fluids is not only helping in head enhancement but also reducing the power consumption of the motor (BHP). Therefore, these fluids provide a higher application range for an ESP used in oil and gas industries without affecting the pump efficiency.

4. Numerical Simulation

Currently for the petroleum industry, it is important to understand how several kinds of ESPs work under multiphase flow conditions; this understanding will greatly influence the production cost of oil and gas. Moreover, it helps the manufacturer to determine the best operational parameters of an ESP. Therefore, CFD alone or in combination with experimental studies has been widely applied in the past to examine the more hidden parameters and extreme operating conditions for an ESP, which cannot be analyzed easily with experimental studies [80–82].

4.1. One-Dimensional (1-D) Two-Phase Modeling

Simple numerical studies for pumps originated late in the 1970s. Several 1-D analytical models were applied by researchers such as Mikielewicz [83], Wilson [84], and Zakem [85], where they have developed some empirical expressions that need some test information. For instance, Zakem et al. [85] have conducted one-dimensional numerical modeling and developed an empirical formula in order to analyze the interaction between gas and liquid. Later in the 1980s, numerical simulations regarding 1-D two-phase flow modelling were carried out, on the basis of a streamline approach, by many researchers such as Furuya [86], Sachdeva [87], Minemura [88], and Sun [89].

Then later in the 1990s, with the development of computer technologies, theoretical prediction of gas-handling performance of an ESP using CFD simulation has become a hot topic for researchers. This is because the flow behavior inside an ESP system is very complex due to the interaction between both the rotating (impeller) and stationery (diffuser) part. Therefore, CFD has played an important role for simulating complex multi-stage pump geometries using several kinds of models such as direct numerical simulation methods (DNS), Reynolds stress (RANS), and large eddy simulation (LES).

4.2. Three-Dimensional (3-D) Two-Phase Flow Modeling

Minmura [90] conducted a 3-D numerical simulation to investigate the effect of inlet gas fraction on the two-phase flow performance of the centrifugal pump, using the bubbly flow model. The authors have observed the formation of the cavity in the impeller flow channel with the increase in gas volume fraction. They have declared that at the point of cavity inception, the pump performance did not change with the increase in gas volume contents. Then, using the finite volume method, a similar numerical approach has been carried out by Pak et al. [91], where they have applied bubbly flow assumptions to investigate the influence of gas entrainment on the pressure variation and performance characteristics of the centrifugal pump. They proposed that the variation in pressure distribution is caused by the gas entrainment in impeller flow channels. Thus, the effect of gas entrainment on

the two-phase handling ability of the single-stage centrifugal pump was investigated by Si et al. [28] under three different IAVFs and flow rates (Table 7).

Table 7. Gas distribution in centrifugal pump impeller flow channel at various flow rates and IAVFs [28].

IAVF	Scale	Flow Rate = 0.6 Q_d	Flow Rate = 0.8 Q_d	Flow Rate = Q_d
1%				
5%				
7%				
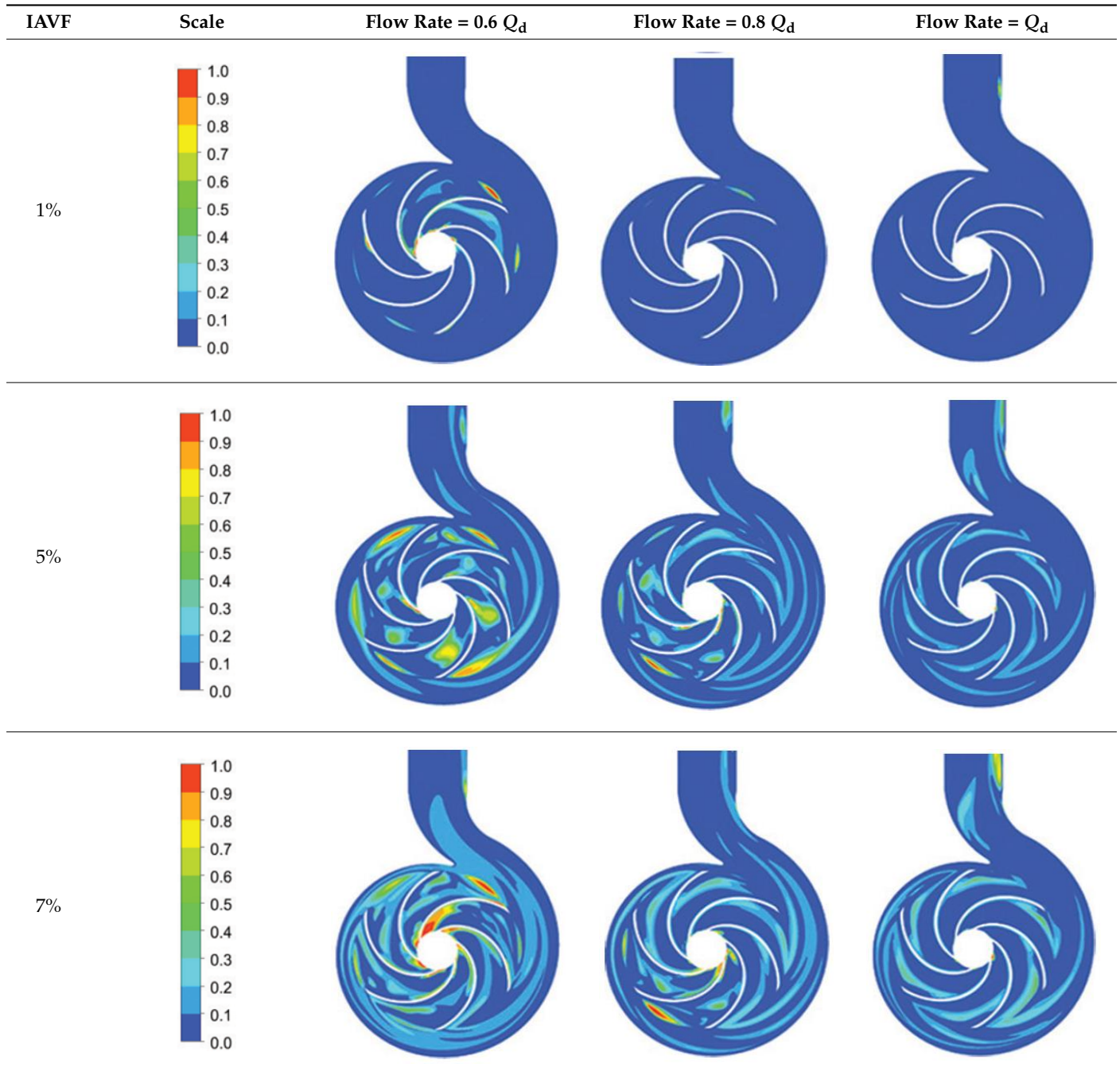
According to Table 7, an obvious and bigger alteration in gas void fraction can be seen in the middle section of the impeller compared to the volute section for all three flow rates and IAVFs. With the increase in IAVFs, air bubbles start to agglomerate on the blade pressure side and are confined more within the impeller flow passage close to the wake region. At 7% of IAVF, bubbles occupied almost 60% of the impeller flow passage for all three flow rates, which caused serious pump performance deterioration.

On the other hand, a decrease in bigger values of gas void fractions was observed with the increase in flow rate, showing that the centrifugal pump is hypersensitive to gas

at lower values of flow rates. These variations alter the whole flow pattern, which in turn causes pump performance degradations. Therefore, the same research team as the present paper has performed the numerical analysis to investigate the different flow patterns in centrifugal-pump-handling gas–liquid two-phase flow [29]. The analysis was performed at a low flow rate by changing the values of IAVF, in order to analyze the internal flow behavior as well as the two-phase handling capability of the pump (see Figure 11a–d). For pure water (IAVF 0%), a strong pre-rotation flow with higher peripheral absolute velocity was observed in the reverse direction. Meanwhile at 7% IAVF, a strong alteration inside the inlet region was observed, impeding the working capability of the centrifugal pump. At this condition, the flow has no or few recirculations because of lower air velocities and pressure gradients. This is why the reverse flow only took place within the initial part of the impeller flow channel.
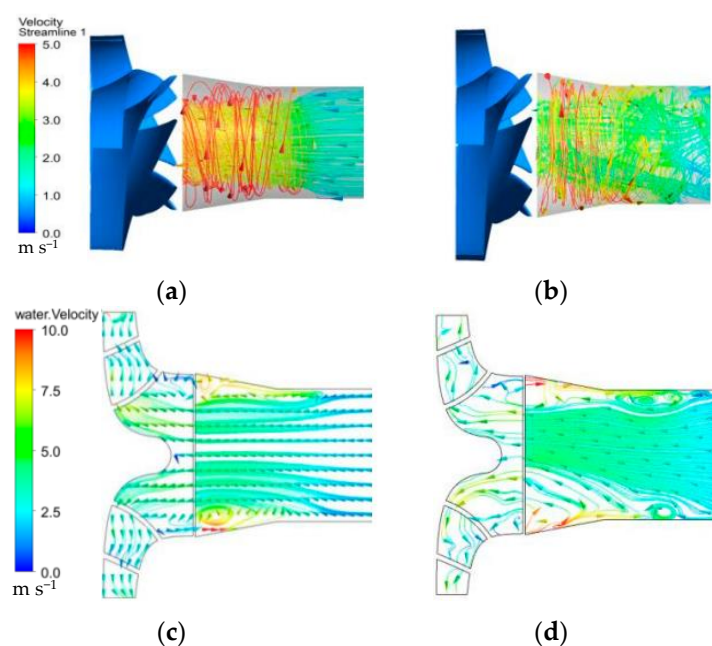

Figure 11. Gas–liquid multiphase patterns within impeller flow channel at designed rotational speed [29], $\varphi = 0.038$: (**a**) IAVF = 0%; (**b**) IAVF = 7%; (**c**) IAVF = 0%; (**d**) IAVF = 7%.

Additionally, the effect of gas entrainment on the ESP's head degradation was studied by Caridad [92], where the two-phase flow-handling ability of an ESP was examined numerically by changing inlet IAVFs. The authors observed that the performance of an ESP decreases as the GVF increases. Their 3-D simulation model was able to predict the gas-pocket formation and pressure distribution in the impeller flow channel. The air pocket was formed on the pressure side of the blade and its size enlarged with the increase in IAVF, causing further head degradation in ESP. The results were obtained at constant bubble size with a diameter of about 0.5 mm.

4.3. Bubble Diameter Effect on Gas-Handling Capability of Pump

Moreover, the aforementioned experimental studies proposed that the gas-pocket formation and bubble agglomeration are strongly dependent on the bubble size and trajectories. Therefore, several researchers, such as Ossia [93], Caridad [94], Barrios [3,95], and Zhu [6,20], have carried out some numerical simulations to investigate the impact of bubble size and location on the gas-handling performance of ESP system. In comparison with each other, Ossia [93] and Caridad [94] have conducted 3-D two-phase flow simulations by employing mixed-flow pump and radial-flow pump, respectively. CFD simulations were carried out by both authors using turbulence and two-fluid models. Caridad [94] has applied a dispersed bubbly flow model with different bubble diameters

(0.1, 0.3, and 0.5 mm) for pump performance prediction, while Ossia's simulations [93] were based on the population balance method and their CFD performance results were in good agreement with the experimental results. Both studies have observed a similar effect of bubble size on pump performance, as shown in Figure 12a. They claimed that the pump performance degradation was caused by the formation of gas pockets that are produced by the agglomeration of bubbles in impeller flow channels. With the increase in bubble size, further deterioration in pump performance was observed because the larger gas pockets were formed, which seriously affected the impeller flow channels. Moreover, both studies have observed different locations of air pockets in the impeller flow passage—Ossia [93] reported the gas-pocket formation on the suction side of the blade, while Caridad [94] reported on the pressure side of the blade as shown in Figure 12b. The difference is caused by the geometrical orientations of pumps that are different in both studies rather than in techniques applied. Notably, similar differences were observed in the test studies, i.e., Tillack [96] observed the bubble agglomeration on the pressure side of the rotor blade whereas Barrios and Prado [17] observed it on the suction side of the rotor blade. In addition to this experimental study, Barrios et al. [3,95] have also conducted two-phase flow numerical simulations on single-stage ESP, where they have established a new model for drag coefficient estimation and bubble-size measurement. Their CFD analysis was in good agreement with the experimental results.
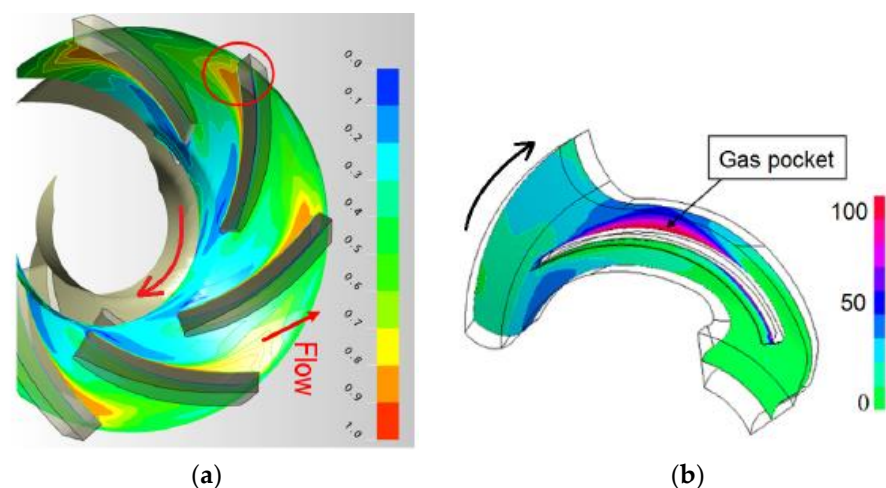

(a)   (b)

Figure 12. Computational fluid dynamics (CFD) results obtained by Ossia [93]. (a) Radial flow pump with GVF = 10% and bubble diameter *d* = 0.5 mm, and Caridad [94] (b) mixed-flow pump with GVF = 30% and *d* = multiple size bubble.

On the contrary, by considering the no-slip GVF and keeping the bubble diameter constant, Zhu et al. [6,20] have performed numerical simulations to predict the multi-phase performance of the submersible pump and observed the similar type of CFD results as Ossia [93] and Caridad [94]. They concluded that the bubble diameter was steadily increased with the increase in no-slip GVF, forming gas pockets, which in turn deteriorate the gas-handling capability of ESP under multiphase flow conditions. Furthermore, Zhu et al. [20] have proposed that the gas-handling ability of an ESP under two-phase flow conditions has improved at higher rotating speeds.

Some unsteady numerical simulations were carried out by Gonzalez [97,98] to analyze the impact of blade–volute interaction on the single-phase performance of the centrifugal pump. They have applied the sliding mesh method for solving Reynolds stress (RANS) equations and found out that a strong unsteady flow is produced by the interaction between blade and volute tongue at off-design conditions, which results in pump performance degradation. Moreover, the transient simulation in combination with the sliding mesh method was helpful in predicting the dynamic flow behavior of the blade and volute

tongue. On the other hand, unsteady multiphase CFD simulations were performed on multi-vane ESP by Marsis [99]. The purpose of this study was to provide some CFD design modification to improve both single and multiphase flow-handling ability of ESP impeller. At inlet GVFs of 24%, an increment in stage pressure was observed in modified design, which was 14% in the case of mono-phase and 23% in the case of multi-phase flow. Then, later in 2019, based on Barrios' experimental data, Zhu et al. [100], have also conducted unsteady CFD simulation to investigate the two-phase flow behavior of an ESP impeller. They have applied and compared two different CFD models: Euler–Euler two-phase model and *k-ε* turbulence model with VOF (volume of fluid) using ANSYS fluent. Their CFD results showed that the Euler–Euler model is better in predicting the flow structures in ESP impeller rather than VOF model. At low gas flow rates, the impeller flow channel was subjected to dispersed bubbly flow, while at higher gas flow rates, the observed flow regime was slug flow leading the gas-pocket formation inside the impeller flow channels. They further claimed that the unsteady two-phase CFD analysis has proven to be the most effective and reliable method to predict the pump performance working under two-phase flow conditions.

4.4. Influence of Viscosity on Two-Phase Performance

The two-phase flow-handling performance of ESP is strongly affected by the fluid viscosity, as proposed in the experimental section. Thus, CFD analysis has also played a significant role in the oil and gas industry for viscosity analysis. Many scholars, such as Shojaeefard [101,102], Sirino [103], Stel [104,105], Zhu [77], Zhang [78], Basaran [106], Ofuchi 2017 [107–110], Valdes [79], have applied different types of CFD techniques to analyze both single-phase and two-phase flow performance of pumps handling viscous fluids. Using the SST *k-ω* turbulence model, Shojaeefard et al. [101,102] have performed CFD simulations to examine the influence of viscous fluids on working capability of centrifugal pumps. On the other hand, using similar two-phase CFD models, the viscosity analysis in single-stage and three-stage ESP systems was carried out by Sirino [103] and Stel [104,105], respectively. Their simulation results were in good agreement with experimental data under a broad value of fluid viscosity.

Furthermore, in 2017, CFD simulation methodology that was similar to Sirino [103] and Stel's [104,105], was applied by Ofuchi [107,108] on three-stage ESP design in order to analyze the effect of viscous Newtonian fluid on ESP performance deterioration. The authors have conducted broad values of fluid viscosity, rotating speed, and flow rate. This study concluded that the frictional losses associated with fluid viscosity have proved to be major contributors for ESP's performance degradation, which was later confirmed by Valdes in 2020 [79].

The aforementioned experimental and numerical analyses have made a great contribution to the prediction and reduction in main parameters (gas involvement, rotational speed, bubble size and fluid viscosity), accountable for performance degradation in ESPs handling two-phase flow conditions. In addition, numerous researchers have provided some design methods that have improved the multiphase flow-handling ability of different types of pumps, discussed in the following section.

5. Design Methods to Increase Two-Phase Flow-Handling Ability of Pumps

Gas handling is defined as the techniques applied in gas–liquid two-phase flow conditions to enhance the pump capability to operate under gassy conditions. In order to design a pump that can produce a higher head and higher efficiency while handling gas, its performance needs to be described in two-phase flow conditions, proposed by Dupoiron [23].

Numerous studies have been conducted regarding the gas-handling ability of the ESP since the late 1980s, and several ESP design models are available that are able to sustain up to 95% of the free gas, using helico-axial pumps [13] and gas separators [14]. The removal of free gas from gas–liquid mixture is not always successful; therefore, the pump must be capable of compressing and moving the gas together with the liquid. The standard ESPs

with radial flow designs can handle about 20% free gas. However, if the free gas content exceeds 20%, the mixed/axial flow designs are applied, which are capable of compressing and pushing the gas to move along the liquid as a homogenous mixture. These designs can handle about 45% of free gas. Furthermore, if the gas volume content exceeds 45%, the different gas separation techniques, in combination with the gas handlers, are used, which can handle up to 95% of free gas, proposed by Bagsi [111]. The design methods used to increase the gas-handling capability of ESP are divided into three main categories that are represented in the subsequent flow chart (see Figure 13) along with their types.
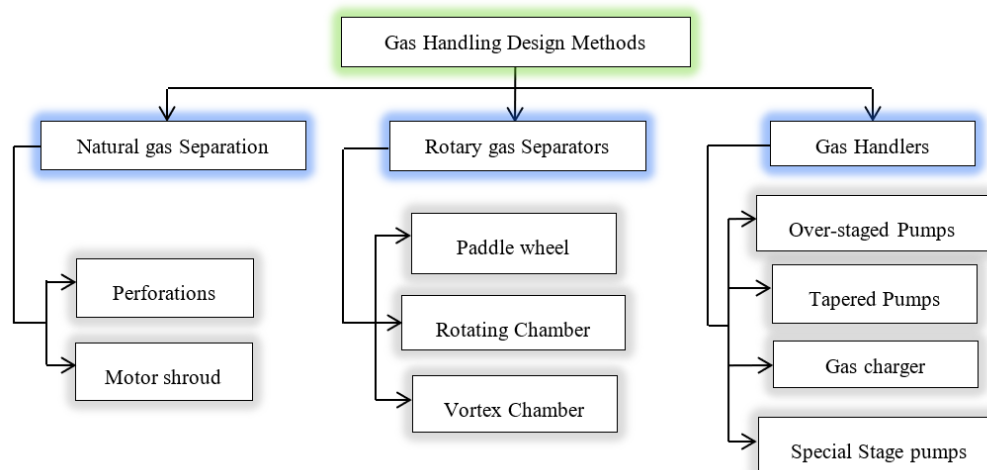

Figure 13. Flow chart of design methods to increase the gas–liquid two-phase handling ability of ESP.

The main concepts behind these three gas-handling design methods are described by Wilson [112] and Bedrin [113] as:

i.   Natural gas separation: The entrance of free gas into the ESP system handling gas–liquid two-phase mixtures should be stopped using natural gas separation techniques.

ii. Rotary gas separation: If the natural gas separation is not sufficient in handling the free gas entrainment into the ESP system, then rotary gas separators (RGSs) should be applied to separate the entered gas before entering into pump.

iii. Gas handlers: If the separation of free gas inside the ESP system is not possible using the aforementioned methods, then gas handlers, alone or in combination with RGS, should be applied, which can carry higher volumes of free gas together with liquid phase without effecting the pump performance.

The natural separation of gas can be achieved either by placing an ESP below the perforations [114] or using a motor shroud along with the perforation method, where the separation between the two phases, gas and liquid, happens due to gravity effect in the casing annulus. Thus, by placing the well below perforations, Kallas and Way [115] have described the natural gas separation method to minimize the free-gas entrainment into the ESP system. The authors proposed that the two-phase flow performance of an ESP was improved, and the pump was capable of handling about 20–30% of inlet GVFs by using these techniques.

Since the gas entrainment in the ESP system is not fully controllable, thus the RGSs [116] have been applied to remove the gas from the casing annulus in the ESP system. The working principle of the different types of RGS (paddle wheel [117], rotating chamber [118], vortex [119]) is based on spinning the gas–liquid two-phase mixture at higher rotational speed in the ESP system, where the separation between the two phases occurs due to different values of centrifugal force working on the gas–liquid particles [8]. Even the separation occurs due to impeller's rotation, but the inducer, which is basically an axial flow pump with lower values of NPSH (net positive suction head), has played an important role in boosting fluid pressure for smooth movement of gas–liquid mixture. The application

of RGSs has significantly improved the gas-handling performance of the ESP system up to 60% [120].

Modern RGSs consist of three main components including (1) an inducer used for boosting the fluid pressure for multiphase mixtures, (2) the guided vanes that are used for modifying the direction of coming fluid into an axial path, and (3) a separator that is responsible for the real separation between gas and liquid with the help of any type of RGS (see Figure 13).

The performance of RGSs is strongly dependent on the geometry of the inducer, GVFs, flow rate, rotational speed, and fluid viscosity [121]; several studies were carried out to investigate the effect of these factors on the separation efficiency of RGS [122–127]. Early investigations on the performance of RGSs were misguided because they considered the separation efficiency to be independent of the effect of gravity in the annulus. However, Alhanati et al. [122,123] were the first ones to find out that the gas separation in the RGS happens in two regions—firstly, in the annulus due to gravity effect (natural gas separation), and secondly, in the separator, which was later justified by Sambangi [124], Lackner [125], and Harun [126]. Additionally, the experiments conducted by Alhanati et al. [122,123] showed that the separation efficiency of RGSs has two regions—higher efficiency (80–100%) and lower efficiency with an abrupt transition. The higher efficiency indicates the cumulative influence of both separator and annulus, while the lower efficiency represents the inefficient behavior of the annulus and inducer. An example of their experimental results is shown in Figure 14. Additionally, all these studies [122,124–126] have covered a wide range of rotational speed, liquid–gas ratios, liquid flow rates, and pressure distributions.
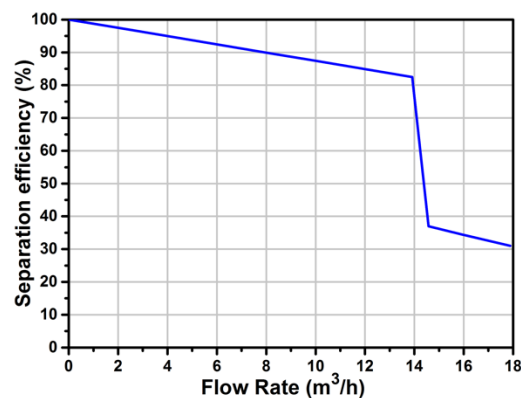

Figure 14. Gas separation efficiency of rotary gas separator (RGS) and the annulus at pump intake pressure of 200 psi [123].

Moreover, Harun et al. [126] have claimed that the separation efficiency of RGSs is greatly influenced by the inducer's head. Therefore, Yanez [128], Harun [129], Suarez [130] and Derakhshan [131] have conducted their studies to analyze the effect of inducer's performance on the separation efficiency of RGSs. Based on experimental approach, Yanez [128] has determined and compared the inducer's head of three RGSs, while Harun [129] has conducted the optimization analysis and proposed that the separation efficiency of RGSs can be increased by optimizing the inducer's geometry. On the other hand, a similar parameter was investigated by Suarez [130] and Derakhshan [131] with the help of numerical simulations. Suarez [130] found out that the inducer's head in two-phase flow conditions is not sufficient to handle frictional losses in the annulus and separator while Derakhshan [131] noticed that the inducer's head can be improved by increasing the number of blades.

In addition, the fluid viscosity analysis regarding RGS's performance was carried out by Lackner et al. [132], where they found out that the fluid viscosity has little effect on the performance of RGSs under two-phase flow conditions because of higher rotational speed in the separators. Separately, the effect of flow rate, viscosity and GVFs on two different RGSs (paddle wheel and vortex) was analyzed numerically by Darbani et al. [121]. It was

evident from their results that at similar conditions, the paddle wheel separator has proven to be more efficient compared to vortex gas separators.

If none of the gas separation techniques are successful in controlling the free gas entrainment into ESP system, then gas handlers, alone or in combination with RGSs, are used that are capable of compressing and moving the gas together with the liquid phase. The most common and initial method regarding gas handlers was to increase the number of stages in the ESPs. The purpose was to improve the smaller head produced by the gas entrainment with a smaller number of stages. The over staging in pumps has significantly improved the gas-handling capability of pumps by eliminating the overload from the upper stages of pumps that is produced by the gas interference. This positive effect of over-staged pumping on the pump performance was justified by Cirilo [34], whose investigations, observations and results are described in Section 3.1, Figure 6. The effect of a similar parameter as Cirilo [34] was also observed by Pessoa [9], but the ESP performance was measured per stage. It was obvious from their analysis that with the increase in flow rate, the surging condition appears to move from upper to down stages, and the average performance of the pump is not valid when observed on a per-stage basis. The main disadvantage in over-stage pumping is that the different stages are operating at different flow rates, which produce many losses in the system and cause failure in the pumping operations.

Therefore, a tapered pump is considered to be a more reliable and energy-efficient gas handler compared to over-staged pump, and its gas-handling capability is dependent on the total flow rate. The main purpose behind the pump tapering was to let the downstream stages compress the gaseous fluids and lower the total fluid rates. The performance of ESPs handling gaseous fluids has increased between 40 and 50% with the help of tapered pumps, observed by Pessoa et al. [35]. They have conducted experimental studies on a tapered pump with a 20-stage axial flow pump, which consists of 104 stages of mixed-flow impeller operating at a design flow rate of 4100 B/D. Crude oil and gas were used as working fluid. They observed that the free GVFs handled by a tapered pump were 50% in the case of light oil and 42% in the case of heavy oil. The authors have further performed gas-locking analysis on the tapered pump and found out that the gas-locking never happened in the pump working with heavy oil.

The efficiency of tapered pumps strongly relies on fluid flow rates [133]. For lower to middle flow rates, the performance of the ESPs handling gaseous fluids has improved because the stages with higher specific speeds are employed at the pump downstream. However, for higher fluid rates, the optimum pump performance cannot be achieved because the stages with higher specific speeds have to be employed at upper stages, resulting as less increment in pump performance [8].

Hence, the gas handlers/chargers are applied in the ESP system that can handle up to 75% of free gas volume fractions [13,134]. A Gas handler is a short-tandem-blade pump in which the higher capacity stages are applied under the main pump. The main idea behind this gas-handling technique is to provide a homogenous mixture of gas and liquid with a smaller bubble size to the main pump by changing the pressure distribution. At this condition, the homogenous gas–liquid mixture enters the main pump as single-phase flow. Advanced gas handlers (AGHs), Poseidon gas handlers (PGHs) [111,135] and multi-vane pumps with extended range (MVPERs) are some of the recently used gas handlers for two-phase mixtures in the ESP. The AGHs and MVPERs are basically modified mixed-flow designs and are capable of handling GVFs of 45% and 70%, respectively, whereas Poseidon gas handlers are modified helico-axial designs that can handle up to 75% of inlet GVFs [111,136,137]. A similar multiphase helico-axial design to Poseidon was applied by [138]; it was able to control up to 97% inlet GVFs. Moreover, detailed information regarding the gas-handling technologies that were being used to pump gas–liquid mixtures is summarized in Table 8 in relation to Hua et al. [139]. Their study also provides information about twin-screw pumps that are able to handle around 100% GVFs, claimed by [140,141]. Even twin-screw pumps can operate under higher GVFs; still, they

have been rarely used in downhole pumping because of their low operating range and erosion sensitive behavior.

Table 8. Present gas-handling technologies for pumping gas–liquid mixtures and important features.

Pump Type	Pumping Mechanism	Max. GVF	Max. Capacity (Gas–liquid)	Max. Pressure	Max. Temperature
Helico-Axial (Poseidon)	Rotating	75%	9000 B/D	-	450 °F
Multi-Vane (Baker Hughes-MVP)	Rotating	70%	18,000 B/D	-	410 °F
Twin-Screw (CAN-K)	Positive displacement	98%	Around 450,000 B/D	Around 3500 psi	662 °F

The gas handlers were followed by the inclusion of special stage pumping devices, in which the gas-handling methods combined with RGSs are used to handle two-phase flow mixtures in ESP. Special stages basically include tapered pumps together with an inducer at the downstream, and special pump stages with lower NPSHs in the middle and normal stages at the upstream. These devices with lower NPSH stages have an advantage of increasing the working capability of pumps by eliminating the surging and gas-blocking phenomena.

The aforementioned studies concerning gas-handling design methods suggest that the installation of ESPs in gas–liquid two-phase flow conditions is no longer a problem. Currently, some design methods are available that, alone or in combination with each other, are able to handle higher volume fractions of gas. This can be achieved by selecting the proper pump stages, gas handlers and RGSs alone or in combination with tapered pumps. The preceding description can be effectively explained through Figure 15, which includes the possible gas-handling design methods, their combinations as well as their application range. Figure 15 is an example of composed data (provided by the Centrilift [142]), extracted by the current authors. It is evident from Figure 15 that the application of gas handlers combined with RGSs has proven to be helpful for further increasing the gas-handling capability of the ESP system.
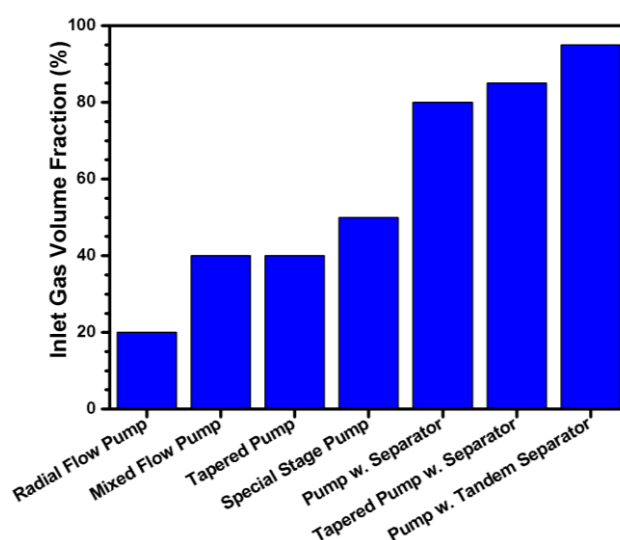

Figure 15. Comparison of different gas-handling techniques used in the ESP system [142].

6. Conclusions

The following conclusions were mainly included:

(1) The recent experimental analysis on ESPs handling multiphase flow (consisting of empirical model and their comparison, flow visualization, bubble size measurements and viscosity analysis) has helped in identifying some major parameters and difficulties that are accountable for pump performance degradation. The gas accumulation, gas-pocket formation and surging initiation mechanism are strongly dependent on the bubble size and trajectories. Bubble size has claimed to be the main parameter responsible for the two-phase performance degradation of ESPs. However, the increase in rotational speed has a positive effect on the pump performance, because the bubble diameter decreased at higher rotational speed, which makes the impeller flow channel more stable.

(2) The comparison among different correlations with our data sets has shown different trends regarding pump performance prediction and surging mechanism. Some empirical models offer good simulation of the data sets in Table 4. However, some of them did not produce any outcomes for our data set, because most of their models were established for high inlet pressure (for example, in the case of Turpin, 344.73 kpa, 689.47 kpa and 1378.95 kpa), no water, but oil and CO_2, multistage arrangement, different rotational speed (compared with our experimental data) and different pump geometries. Therefore, these empirical models become specific and valid for the pump types evaluated. This is the reason why most researchers performed more specific research using much simpler arrangements, such as centrifugal or mixed-flow single stages, in order to get more local flow features.

(3) The visualization techniques have played a satisfactory role in examining the unsteady internal flow behavior of the fluid and different flow patterns inside the rotating ESPs. However, the complete two-phase flow phenomena, responsible for pump performance degradation, are still difficult to visualize because of the complex geometry of ESP stages having several impeller and diffusers. Although the CFD-based numerical simulations, alone or in combination with experimental studies, have been used as an alternate to analyze the two-phase flow, its reliability and accuracy are still questioned.

(4) Gas-handling design methods have successfully increased the two-phase handling ability of ESPs either by stopping the entrance of free gas into the pump system (natural gas separation) or removing the entered gas with the help of RGSs alone or combined with gas handlers. The application of gas handlers combined with RGSs has proven to be very useful for increasing the gas-handling capability of the ESP system up to 95%. This paper has an individuality in describing the complete mechanism of all the gas-handling techniques.

7. Future Recommendations

Regarding future recommendations, the author suggests that the macro lens (special method applied by Besagni, and Inzoli [143] for image processing) should be used while performing visualization experiments that could provide quantitative measurements for the bubble diameter distribution and trajectories.

Since the annular flow condition causes severe degradation in pump performance, the CFD-based numerical simulations must consider both bubbly and annular flow conditions in order to achieve better outcomes. These characteristics may arise at inlet flow conditions, which are dependent on the rotational speed, flow coefficient and experimental setup.

The authors presumed that the gas-handling capability of the ESP could be improved by the reduction in density ratio because it is very sensitive to gas–liquid two-phase interaction and flow separation mechanism. Therefore, our further research may include the test at higher suction pressure in order to examine the effect of density ratio reduction on the gas-handling capability of ESP.

References

1. Takacs, G. Chapter 1—Introduction. In *Electrical Submersible Pumps Manual*, 2nd ed.; Takacs, G., Ed.; Gulf Professional Publishing: Houston, TX, USA, 2017; pp. 1–10.
2. Brookbank, E. *Electric Submersible Pumps—The First Sixty Years*; European ESP Workshop: London, UK, 1988.
3. Barrios, L.J. Visualization and Modeling of Multiphase Performance Inside an Electrical Submersible Pump. Ph.D. Thesis, The University of Tulsa, Tulsa, OK, USA, 2007.
4. Barrios, L.; Rojas, M.; Monteiro, G.; Sleight, N. Brazil field experience of ESP performance with viscous emulsions and high gas using multi-vane pump MVP and high power ESPs. In Proceedings of the SPE Electric Submersible Pump Symposium: The Woodlands, Richardson, TX, USA, 24–28 April 2017; Society of Petroleum Engineers: Richardson, TX, USA, 2017.
5. Ladopoulos, E. Four-dimensional Petroleum Exploration & Non-linear ESP Artificial Lift by Multiple Pumps for Petroleum Well Development. *Univ. J. Hydr.* **2015**, *1*, 14.
6. Zhu, J.; Zhang, H.-Q. CFD simulation of ESP performance and bubble size estimation under gassy conditions. In Proceedings of the SPE Annual Technical Conference and Exhibition, Amsterdam, The Netherlands, 27–29 October 2014; Society of Petroleum Engineers: Richardson, TX, USA, 2014.
7. Banjar, H.; Gamboa, J.; Zhang, H.-Q. Experimental study of liquid viscosity effect on two-phase stage performance of electrical submersible pumps. In Proceedings of the SPE Annual Technical Conference and Exhibition, New Orleans, LA, USA, 30 September–2 October 2013; Society of Petroleum Engineers: Richardson, TX, USA, 2013.
8. Takacs, G. Chapter 4—Use of ESP Equipment in Special Conditions. In *Electrical Submersible Pumps Manual*; Takacs, G., Ed.; Gulf Professional Publishing: Boston, MA, USA, 2009; pp. 119–186.
9. Pessoa, R.; Prado, M. Two-phase flow performance for electrical submersible pump stages. *SPE Prod. Facil.* **2003**, *18*, 13–27. [CrossRef]
10. Estevam, V. A Phenomenological Analysis about Centrifugal Pump in Two-Phase Flow Operation. Ph.D. Thesis, Universidade Estadual de Campinas, Campinas, Brazil, 2002.
11. Gamboa, J. Prediction of the Transition in Two-Phase Performance of an Electrical Submersible Pump. Ph.D. Dissertation, University of Tulsa, Tulsa, OK, USA, 2008.
12. Zhou, D.; Sachdeva, R. Simple model of electric submersible pump in gassy well. *J. Pet. Sci. Eng.* **2010**, *70*, 204–213. [CrossRef]
13. Camilleri, L.A.; Brunet, L.; Segui, E. Poseidon Gas Handling Technology: A Case Study of Three ESP Wells in the Congo. In Proceedings of the SPE Middle East Oil and Gas Show and Conference, Manama, Bahrain, 25–28 September 2011.
14. Rahime, F.; Sakr, K.; Areekat, M.; Suryadi, R. Application of the Gas Handlers in KOC. In Proceedings of the SPE Middle East Oil and Gas Show and Conference, Manama, Bahrain, 10–13 March 2013.
15. Murakami, M.; Minemura, K. Effects of entrained air on the performance of a centrifugal pump: 1st report, performance and flow conditions. *Bull. JSME* **1974**, *17*, 1047–1055. [CrossRef]
16. Sekoguchi, K.; Takada, S.; Kanemori, Y. Study of air-water two-phase centrifugal pump by means of electric resistivity probe technique for void fraction measurement: 1st report, measurement of void fraction distribution in a radial flow impeller. *Bull. JSME* **1984**, *27*, 931–938. [CrossRef]
17. Barrios, L.; Prado, M.G. Experimental visualization of two-phase flow inside an electrical submersible pump stage. *J. Energy Resour. Technol.* **2011**, *133*. [CrossRef]
18. Schobeiri, M. *Turbomachinery Flow Physics and Dynamic Performance*; Springer: Berlin/Heidelberg, Germany, 2012.

19. Gülich, J.F. Pump types and performance data. In *Centrifugal Pumps*; Springer: Berlin/Heidelberg, Germany, 2014; pp. 43–78.

20. Zhu, J.; Zhang, H.-Q. Numerical study on electrical-submersible-pump two-phase performance and bubble-size modeling. *SPE Prod. Oper.* **2017**, *32*, 267–278. [CrossRef]

21. Shi, Y.; Zhu, H.; Zhang, J.; Zhang, J.; Zhao, J. Experiment and numerical study of a new generation three-stage multiphase pump. *J. Pet. Sci. Eng.* **2018**, *169*, 471–484. [CrossRef]

22. De Salis, J.; De Marolles, C.; Falcimaigne, J.; Durando, P. Multiphase pumping-operation & control. In Proceedings of the SPE Annual Technical Conference and Exhibition, Denver, CO, USA, 6–9 October 1996. [CrossRef]

23. Dupoiron, M.A.N. The Effect of Gas on Multi-Stage Mixed-Flow Centrifugal Pumps. Ph.D. Thesis, University of Cambridge, Cambridge, UK, 2018.

24. Truesdell, C.; Euler, L. *The Rational Mechanics of Flexible or Elastic Bodies, 1638–1788: Introduction to Leonhardi Euleri Opera Omnia Vol X Et XI Seriei Secundae*; Orell Füssli: Zürich, Switzerland, 1960; Volume 11.

25. Si, Q.; Ali, A.; Yuan, J.; Fall, I.; Muhammad Yasin, F. Flow-Induced Noises in a Centrifugal Pump: A Review. *Sci. Adv. Mater.* **2019**, *11*, 909–924. [CrossRef]

26. Zhu, J.; Zhang, H.-Q. A review of experiments and modeling of gas-liquid flow in electrical submersible pumps. *Energies* **2018**, *11*, 180.

27. Si, Q.; Bois, G.; Zhang, K.; Yuan, J. Air-water two-phase flow experimental and numerical analysis in a centrifugal pump. In Proceedings of the 12th European Conference on Turbomachinery, Fluid Dynamics and Thermodynamics, Stockholm, Sweden, 3–7 April 2017; pp. 3–7.

28. Si, Q.; Cui, Q.; Zhang, K.; Yuan, J.; Bois, G. Investigation on centrifugal pump performance degradation under air-water inlet two-phase flow conditions. *La Houille Blanche* **2018**, 41–48. [CrossRef]

29. Si, Q.; Bois, G.; Jiang, Q.; He, W.; Ali, A.; Yuan, S. Investigation on the Handling Ability of Centrifugal Pumps under Air–Water Two-Phase Inflow: Model and Experimental Validation. *Energies* **2018**, *11*, 3048. [CrossRef]

30. Si, Q.; Cui, Q.; Shouqi, Y.U.A.N.; Zhang, K.; Cao, R.; Tang, Y. Influence of inlet gas volume fraction on similarity law in centrifugal pumps under gas-liquid Two-phase Condition. In *Transactions of the Chinese Society for Agricultural Machinery*; Editorial Office of Transactions of the Chinese Society of Agricultural Engineering: Beijing, China, 2018.

31. Jiang, Q.; Heng, Y.; Liu, X.; Zhang, W.; Bois, G.; Si, Q. A review of design considerations of centrifugal pump capability for handling inlet gas-liquid two-phase flows. *Energies* **2019**, *12*, 1078. [CrossRef]

32. Lea, J.F.; Bearden, J. Effect of gaseous fluids on submersible pump performance. *J. Pet. Technol.* **1982**, *34*, 2922–2930. [CrossRef]

33. Turpin, J.L.; Lea, J.F.; Bearden, J.L. Gas-liquid flow through centrifugal pumps-Correlation of data. In Proceedings of the 3rd International Pump Symposium, Houston, TX, USA, 20–22 May 1986. [CrossRef]

34. Cirilo, R. Air-Water Flow through Electric Submersible Pumps. Ph.D. Thesis, University of Tulsa, Department of Petroleum Engineering, Tulsa, OK, USA, 1998.

35. Pessoa, R.; Machado, M.; Robles, J.; Escalante, S.; Henry, J. Tapered Pump Experimental Tests with Light and Heavy Oil in PDVSA INTEVEP Field Laboratory. In Proceedings of the SPE-ESP Workshop (April 1999), Houston, TX, USA, 28–30 April 1999.

36. Romero, M. An Evaluation of an Electrical Submersible Pumping System for High GOR Wells. Ph.D. Thesis, University of Tulsa, Tulsa, OK, USA, 1999.

37. Sachdeva, R. Two-Phase Flow through Electric Submersible Pumps. Ph.D. Thesis, University of Tulsa, Tulsa, OK, USA, 1988.

38. Sachdeva, R.; Doty, D.; Schmidt, Z. In Performance of Axial Electric Submersible Pumps in a Gassy Well. In Proceedings of the SPE Rocky Mountain Regional Meeting, Casper, Wyoming, 18–21 May 1992.

39. Duran, J.; Prado, M.G. ESP stages air-water two-phase performance—Modeling and experimental data. SPE 120628. In Proceedings of the 2004 SPE ESP Workshop, Houston, TX, USA, 28–30 April 2004.

40. Salehi, E. ESP Performance in Two-Phase FLOW through Mapping and Surging Tests at Various Rotational Speeds and Intake Pressures. Master's Thesis, University of Tulsa, Tulsa, OK, USA, 2012.

41. Mohammadzaheri, M.; Tafreshi, R.; Khan, Z.; Franchek, M.; Grigoriadis, K. In Modelling of Petroleum Multiphase Fluids in ESP an Intelligent Approach. In Proceedings of the Offshore Mediterranean Conference and Exhibition, Ravenna, Italy, 25–27 March 2015.

42. Mohammadzaheri, M.; Tafreshi, R.; Khan, Z.; Ziaiefar, H.; Ghodsi, M.; Franchek, M.; Grigoriadis, K. Modelling of electrical submersible pumps for petroleum multiphase fluids, an intelligent approach supported by a critical review and experimental results. *J. Eng. Res.* **2019**, *16*, 77–86. [CrossRef]

43. Zhu, J.; Guo, X.; Liang, F.; Zhang, H.-Q. Experimental study and mechanistic modeling of pressure surging in electrical submersible pump. *J. Nat. Gas Sci. Eng.* **2017**, *45*, 625–636. [CrossRef]

44. Zhu, J.; Zhang, J.; Cao, G.; Zhao, Q.; Peng, J.; Zhu, H.; Zhang, H.-Q. Modeling flow pattern transitions in electrical submersible pump under gassy flow conditions. *J. Pet. Sci. Eng.* **2019**, *180*, 471–484. [CrossRef]

45. Mohammadzaheri, M.; Tafreshi, R.; Khan, Z.; Ghodsi, M.; Franchek, M.; Grigoriadis, K. Modelling of petroleum multiphase flow in electrical submersible pumps with shallow artificial neural networks. *Ships Offshore Struct.* **2020**, *15*, 174–183. [CrossRef]

46. Si, Q.; Zhang, H.; Bois, G.; Zhang, J.; Cui, Q.; Yuan, S. Experimental investigations on the inner flow behavior of centrifugal pumps under inlet air-water two-phase conditions. *Energies* **2019**, *12*, 4377. [CrossRef]

47. Gamboa, J.; Prado, M. Review of electrical-submersible-pump surging correlation and models. *SPE Prod. Oper.* **2011**, *26*, 314–324. [CrossRef]

48. Murakami, M.; Minemura, K. Effects of entrained air on the performance of centrifugal pumps: 2nd report, effects of number of blades. *Bull. JSME* **1974**, *17*, 1286–1295. [CrossRef]
49. Patel, B. Investigations into the two-phase flow behavior of centrifugal pumps. *Proc. Polyph. Flow Turbomach. ASME* **1978**, 79–100.
50. Kim, J.; Duffey, R.; Belloni, P. On centrifugal pump head degradation in two-phase flow. In *Design Methods for Two-Phase Flow in Turbomachinery*; ASME: New York, NY, USA, 1985.
51. Furukawa, A.; Shirasu, S.-I.; Sato, S. Experiments on air-water two-phase flow pump impeller with rotating-stationary circular cascades and recirculating flow holes. *JSME Int. J. Ser. B Fluids Therm. Eng.* **1996**, *39*, 575–582. [CrossRef]
52. Sato, S.; Furukawa, A.; Takamatsu, Y. Air-water two-phase flow performance of centrifugal pump impellers with various blade angles. *JSME Int. J. Ser. B Fluids Therm. Eng.* **1996**, *39*, 223–229. [CrossRef]
53. Andras, E. Two Phase Flow Centrifugal Pump Performance. Ph.D. Thesis, Idaho State University, Pocatello, ID, USA, 1997.
54. Takemura, T.; Kato, H.; Kanno, H.; Okamoto, H.; Aoki, M.; Goto, A.; Egashira, K.; Shoda, S. Development of rotordynamic multiphase pump: The first report. In Proceedings of the International Conference on Offshore Mechanics and Arctic Engineering, Vancouver, BC, Canada, 13–17 April 1997; pp. 201–208.
55. Thum, D.; Hellmann, D.; Sauer, M. Influence of the Patterns of Liquid-Gas Flows on Multiphase-Pumping of Radial Centrifugal Pumps. In Proceedings of the 5th North American Conference on Multiphase Technology, Banff, AB, Canada, 31 May–2 June 2006; pp. 79–90.
56. Izturitz, D.L.; Kenyery, F. *Effect of Bubble Size on an ESP Performance Handling Two-Phase Flow Conditions*; UBS-LABCEM Publication: Caracas, Venezuela, 2007; pp. 931–939.
57. Schäfer, T.; Bieberle, A.; Neumann, M.; Hampel, U. Application of gamma-ray computed tomography for the analysis of gas holdup distributions in centrifugal pumps. *Flow Meas. Instrum.* **2015**, *46*, 262–267. [CrossRef]
58. Schäfer, T.; Neumann-Kipping, M.; Bieberle, A.; Bieberle, M.; Hampel, U. Ultrafast X-Ray Computed Tomography Imaging for Hydrodynamic Investigations of Gas–Liquid Two-Phase Flow in Centrifugal Pumps. *J. Fluids Eng.* **2020**, *142*. [CrossRef]
59. Shao, C.; Li, C.; Zhou, J. Experimental investigation of flow patterns and external performance of a centrifugal pump that transports gas-liquid two-phase mixtures. *Int. J. Heat Fluid Flow* **2018**, *71*, 460–469. [CrossRef]
60. Cubas, J.M.; Stel, H.; Ofuchi, E.M.; Neto, M.A.M.; Morales, R.E. Visualization of two-phase gas-liquid flow in a radial centrifugal pump with a vaned diffuser. *J. Pet. Sci. Eng.* **2020**, *187*, 106848. [CrossRef]
61. Stel, H.; Ofuchi, E.M.; Sabino, R.H.; Ancajima, F.C.; Bertoldi, D.; Marcelino Neto, M.A.; Morales, R.E. Investigation of the motion of bubbles in a centrifugal pump impeller. *J. Fluids Eng.* **2019**, *141*. [CrossRef]
62. Zhang, J.; Cai, S.; Li, Y.; Zhu, H.; Zhang, Y. Visualization study of gas–liquid two-phase flow patterns inside a three-stage rotodynamic multiphase pump. *Exp. Therm. Fluid Sci.* **2016**, *70*, 125–138. [CrossRef]
63. Verde, W.M.; Biazussi, J.L.; Sassim, N.A.; Bannwart, A.C. Experimental study of gas-liquid two-phase flow patterns within centrifugal pumps impellers. *Exp. Therm. Fluid Sci.* **2017**, *85*, 37–51. [CrossRef]
64. Trevisan, F.E. Modeling and Visualization of Air and Viscous Liquid in Electrical Submersible pump. Ph.D. Thesis, University of Tulsa, Tulsa, OK, USA, 2009.
65. Ippen, A.T. The influence of viscosity on centrifugal pump performance. *Trans. ASME* **1946**, *68*, 823–848.
66. Institute, H. *Tentative Standards of Hydraulic Institute: Charts for the Determination of Pump Performance when Handling Viscous Liquids*; The Institute: New York, NY, USA, 1948. [CrossRef]
67. Stepanoff, A.J. *Centrifugal and Axial Flow Pumps. Theory, Design, and Application*; John Wiley & Sons: Hoboken, NJ, USA, 1957.
68. Gülich, J. Pumping highly viscous fluids with centrifugal pumps—Part 1. *World Pumps* **1999**, *1999*, 30–34. [CrossRef]
69. Gülich, J. Pumping highly viscous fluids with centrifugal pumps—Part 2. *World Pumps* **1999**, *1999*, 39–42. [CrossRef]
70. Añez, D.; Kenyery, F.; Escalante, S.I.; Teran, V.M. ESP's Performance with Two-Phase and Viscous Flow. *Proc. ETCE* **2001**, 5–7.
71. Turzo, Z.; Takacs, G.; Zsuga, J. Equations correct centrifugal pump curves for viscosity. *Oil Gas J.* **2000**, *98*, 57.
72. Amaral, G.; Estevam, V.; Franca, F.A. On the influence of viscosity on ESP performance. *SPE Prod. Oper.* **2009**, *24*, 303–311. [CrossRef]
73. Solano, E.A. Viscous Effects on the Performance of Electro Submersible Pumps (ESP's). Master's Thesis, University of Tulsa, Tulsa, OK, USA, 2009.
74. Trevisan, F.E.; Prado, M. Experimental Investigation of the Viscous Effect on Two-Phase-Flow Patterns and Hydraulic Performance of Electrical Submersible Pumps. *J. Can. Pet. Technol.* **2011**, *50*, 45–52. [CrossRef]
75. Bannwart, A.C.; Estevam, V.; Paternost, G.M. Experimental Study of Centrifugal Pump Handling Viscous Fluid and Two-Phase Flow. In Proceedings of the SPE Artificial Lift Conference-Americas, Cartagena, Colombia, 21–22 May 2013.
76. Paternost, G.M.; Bannwart, A.C.; Estevam, V. Experimental study of a centrifugal pump handling viscous fluid and two-phase flow. *SPE Prod. Oper.* **2015**, *30*, 146–155. [CrossRef]
77. Zhu, J.; Banjar, H.; Xia, Z.; Zhang, H.-Q. CFD simulation and experimental study of oil viscosity effect on multi-stage electrical submersible pump (ESP) performance. *J. Pet. Sci. Eng.* **2016**, *146*, 735–745. [CrossRef]
78. Zhang, J. Experiments, CFD Simulation and Modeling of ESP Performance under Viscous Fluid Flow Conditions. Master's Thesis, The University of Tulsa, Tulsa, OH, USA, 2017.
79. Valdés, J.P.; Becerra, D.; Rozo, D.; Cediel, A.; Torres, F.; Asuaje, M.; Ratkovich, N. Comparative analysis of an electrical submersible pump's performance handling viscous Newtonian and non-Newtonian fluids through experimental and CFD approaches. *J. Pet. Sci. Eng.* **2020**, *187*, 106749. [CrossRef]

80. Anderson, J.D.; Wendt, J. *Computational Fluid Dynamics*; Springer: Berlin/Heidelberg, Germany, 1995; Volume 206.

81. Li, W.; Awais, M.; Ru, W.; Shi, W.; Ajmal, M.; Uddin, S.; Liu, C. Review of Sensor Network-Based Irrigation Systems Using IoT and Remote Sensing. *Adv. Meteorol.* **2020**, *2020*. [CrossRef]

82. Si, Q.; Shen, C.; Ali, A.; Cao, R.; Yuan, J.; Wang, C. Experimental and numerical study on gas-liquid two-phase flow behavior and flow induced noise characteristics of radial blade pumps. *Processes* **2019**, *7*, 920. [CrossRef]

83. Mikielewicz, J.; Wilson, D.G.; Chan, T.-C.; Goldfinch, A.L. A method for correlating the characteristics of centrifugal pumps in two-phase flow. *J. Fluids Eng.* **1978**, *100*, 395–409. [CrossRef]

84. Wilson, D.G.; Chan, T.; Manzano-Ruiz, J. *Analytical Models and Experimental Studies of Centrifugal-Pump Performance in Two-Phase Flow*; Report No. EPRI NP-677; MIT: Cambridge, MA, USA, 1979.

85. Zakem, S. Determination of gas accumulation and two-phase slip velocity ratio in a rotating impeller. In *ASME, Polyphase Flow and Transportation Technology*; ASME: New York, NY, USA, 1980; Volume 167–173.

86. Furuya, O. An analytical model for prediction of two-phase (noncondensable) flow pump performance. *J. Fluids Eng.* **1985**, *107*, 139–147. [CrossRef]

87. Sachdeva, R.; Doty, D.; Schmidt, Z. Performance of electric submersible pumps in gassy wells. *SPE Prod. Facil.* **1994**, *9*, 55–60. [CrossRef]

88. Minemura, K.; Uchiyama, T.; Shoda, S.; Egashira, K. Prediction of air-water two-phase flow performance of a centrifugal pump based on one-dimensional two-fluid model. *J. Fluids Eng.* **1998**, *120*, 327–334. [CrossRef]

89. Sun, D.; Prado, M. Modeling gas-liquid head performance of electrical submersible pumps. In Proceedings of the ASME Pressure Vessels and Piping Conference, San Diedo, CA, USA, 25–29 July 2004; pp. 63–71.

90. Minemura, K.; Uchiyama, T. Three-dimensional calculation of air-water two-phase flow in a centrifugal pump based on a bubbly flow model with fixed cavity. *JSME Int. J. Ser. B Fluids Therm. Eng.* **1994**, *37*, 726–735. [CrossRef]

91. Pak, E.; Lee, J. Performance and pressure distribution changes in a centrifugal pump under two-phase flow. *Proc. Inst. Mech. Eng. Part A J. Power Energy* **1998**, *212*, 165–171. [CrossRef]

92. Caridad, J.; Kenyery, F. CFD analysis of electric submersible pumps (ESP) handling two-phase mixtures. *J. Energy Resour. Technol.* **2004**, *126*, 99–104. [CrossRef]

93. Ossia, S.; Godeluck, J. *Gas-Liquid Flow CFD Study of SN8500*; Internal Report: GeMS 100318644; Schlumberger Ltd.: Houston, TX, USA, 2006.

94. Caridad, J.; Asuaje, M.; Kenyery, F.; Tremante, A.; Aguillón, O. Characterization of a centrifugal pump impeller under two-phase flow conditions. *J. Pet. Sci. Eng.* **2008**, *63*, 18–22. [CrossRef]

95. Barrios, L.; Prado, M.G.; Kenyery, F. CFD Modeling Inside an Electrical Submersible Pump in Two-Phase Flow Condition. In Proceedings of the Fluids Engineering Division Summer Meeting, Vail, CO, USA, 2–6 August 2009; pp. 457–469.

96. Tillack, P. Förderverhalten von Kreiselpumpen bei viskosen, gasbeladenen Flüssigkeiten. *Phd Diss. Tu Kaiserslaut.* **1998**.

97. Gonzalez, J.; Fernandez, J.N.; Blanco, E.; Santolaria, C. Numerical simulation of the dynamic effects due to impeller-volute interaction in a centrifugal pump. *J. Fluids Eng.* **2002**, *124*, 348–355. [CrossRef]

98. González, J.; Santolaria, C. Unsteady flow structure and global variables in a centrifugal pump. *J. Fluids Eng.* **2006**, *128*, 937–946. [CrossRef]

99. Marsis, E.; Pirouzpanah, S.; Morrison, G. CFD-based design improvement for single-phase and two-phase flows inside an electrical submersible pump. In Proceedings of the Fluids Engineering Division Summer Meeting, Incline Village, NV, USA, 7–11 July 2013.

100. Zhu, J.; Zhu, H.; Zhang, J.; Zhang, H.-Q. A numerical study on flow patterns inside an electrical submersible pump (ESP) and comparison with visualization experiments. *J. Pet. Sci. Eng.* **2019**, *173*, 339–350. [CrossRef]

101. SHOJAEIFARD, M.; Boyaghchi, F.; Ehghaghi, M. Experimental study and three-dimensional numerical flow simulation in a centrifugal pump when handling viscous fluids. *IUST Int. J. Eng. Sci.* **2006**, *17*, 53–60.

102. Shojaeefard, M.; Tahani, M.; Ehghaghi, M.; Fallahian, M.; Beglari, M. Numerical study of the effects of some geometric characteristics of a centrifugal pump impeller that pumps a viscous fluid. *Comput. Fluids* **2012**, *60*, 61–70. [CrossRef]

103. Sirino, T.; Stel, H.; Morales, R.E. Numerical study of the influence of viscosity on the performance of an electrical submersible pump. In Proceedings of the Fluids Engineering Division Summer Meeting, Incline Village, NV, USA, 7–11 July 2013; American Society of Mechanical Engineers Digital Collection: Incline Village, NV, USA, 2013.

104. Stel, H.; Sirino, T.; Prohmann, P.R.; Ponce, F.; Chiva, S.; Morales, R.E. CFD investigation of the effect of viscosity on a three-stage electric submersible pump. In Proceedings of the 4th Joint US-European Fluids Engineering Division Summer Meeting Collocated with the ASME 2014 12th International Conference on Nanochannels, Microchannels, and Minichannels, Chicago, IL, USA, 3–7 August 2014.

105. Stel, H.; Sirino, T.; Ponce, F.J.; Chiva, S.; Morales, R.E. Numerical investigation of the flow in a multistage electric submersible pump. *J. Pet. Sci. Eng.* **2015**, *136*, 41–54. [CrossRef]

106. Basaran, B. CFD Simulation for the Erosion on Electrical Submersible Pump Due to Viscosity and Air presence. Master's Thesis, Texas A & M University, College Station, TX, USA, 2017.

107. Ofuchi, E.M.; Stel, H.; Sirino, T.; Vieira, T.S.; Ponce, F.J.; Chiva, S.; Morales, R.E. Numerical investigation of the effect of viscosity in a multistage electric submersible pump. *Eng. Appl. Comput. Fluid Mech.* **2017**, *11*, 258–272. [CrossRef]

108. Ofuchi, E.; Stel, H.; Vieira, T.; Ponce, F.; Chiva, S.; Morales, R. Study of the effect of viscosity on the head and flow rate degradation in different multistage electric submersible pumps using dimensional analysis. *J. Pet. Sci. Eng.* **2017**, *156*, 442–450. [CrossRef]

109. Ofuchi, E.; Cubas, J.; Stel, H.; Dunaiski, R.; Vieira, T.; Morales, R. A new model to predict the head degradation of centrifugal pumps handling highly viscous flows. *J. Pet. Sci. Eng.* **2020**, *187*, 106737. [CrossRef]

110. Awais, M.; Li, W.; Arshad, A.; Haydar, Z.; Yaqoob, N.; Hussain, S. Evaluating removal of tar contents in syngas produced from downdraft biomass gasification system. *Int. J. Green Energy* **2018**, *15*, 724–731. [CrossRef]

111. Bagci, A.S.; Kece, M.M.; Rivero, N.; Delida, J. Challenges of Using Electrical Submersible Pump (ESP) in High Free Gas Applications. In Proceedings of the International Oil and Gas Conference and Exhibition in China, Beijing, China, 8–10 June 2010; Society of Petroleum Engineers: Beijing, China, 2010; p. 131760.

112. Wilson, B. There's No Free Lunch, Pumping Two Phase Fluids with ESP. In Proceedings of the SPE Gulf Coast Section Electric Submersible Pump Workshop, Houston, TX, USA, 30 April–2 May 2003.

113. Bedrin, V.; Khasanov, M.; Khabibullin, R.; Krasnov, V.; Pashali, A.; Litvinenko, K.; Elichev, V.; Prado, M. High GLR ESP Technologies Comparison, Field Test Results (Russian). In Proceedings of the SPE Russian Oil and Gas Technical Conference and Exhibition, Moscow, Russia, 28–30 October 2008; p. 117414.

114. Wilson, B.; Mack, J.; Foster, D. Operating electrical submersible pumps below the perforations. *SPE Prod. Facil.* **1998**, *13*, 141–145. [CrossRef]

115. Kallas, P.; Way, K. An Electrical Submergible Pumping System for High GOR Wells. In Proceedings of the SPE Electrical Submergible Pump Workshop, Houston, TX, USA, 26 April 1995.

116. Lee, L.C.; Tyagi, M.K.; Furnas, M.W.; Traylor, F.T. Liquid-Gas Separator Apparatus. U.S. Patent 4,481,020, 6 November 1984.

117. Bunnelle, P.R. Liquid-Gas Separator Unit. U.S. Patent 3,887,342, 3 June 1975.

118. Tuzson, J.J. Separator. U.S. Patent 4,088,459, 9 May 1978.

119. Enegess, D.N. Vortex Gas Separator. U.S. Patent 4,162,901, 31 July 1979.

120. Kobylinski, L.; Taylor, F.; Brienan, J. Development and field test results of an efficient downhole centrifugal gas separator. *J. Pet. Technol.* **1985**, *37*, 1295–1304. [CrossRef]

121. Darbani, S.; Riasi, A.; Nejat, A. The parametric study of an electrical submersible pump rotary gas separator under two-phase flow condition. *Energy Equip. Syst.* **2015**, *3*, 33–44.

122. Alhanati, F.J.S. Bottomhole Gas Separation Efficiency in Electrical Submersible Pump Installations. Ph.D. Thesis, University of Tulsa, Tulsa, OK, USA, 1993.

123. Alhanati, F.; Doty, D. A simple model for the efficiency of rotary separators. In Proceedings of the SPE Annual Technical Conference and Exhibition, New Orleans, LA, USA, 25–28 September 1994.

124. Sambangi, S.R. Gas Separation Efficiency in Electrical Submersible Pump Installations with Rotary Gas Separators. Ph.D. Thesis, University of Tulsa, Tulsa, OK, USA, 1994.

125. Lackner, G. The Effect of Viscosity on Downhole Gas Separation in a Rotary Gas Separator. Ph.D. Thesis, Tulsa University, Tulsa, OK, USA, 1997.

126. Harun, A.F. The Effect of Inducer Performance on the Efficiency of the ESP Rotary Gas Separator. Ph.D. Dissertation, Tulsa University, Tulsa, OK, USA, 2000.

127. Awais, M.; Li, W.; Munir, A.; Omar, M.M.; Ajmal, M. Experimental investigation of downdraft biomass gasifier fed by sugarcane bagasse and coconut shells. *Biomass Convers. Biorefinery* **2020**, 1–16. [CrossRef]

128. Yanez, R.; Escalante, S.I.; Pessoa, R.; Pena, M. *Experimental Test to Obtain Inducer Curve of Rotary Gas Separators*; Technical Report Intevep, INT-3967; Intevep: Los Teques, Venezuela, 1997.

129. Harun, A.; Prado, M.; Doty, D. Design Optimization of a Rotary Gas Separator in ESP Systems. In Proceedings of the SPE Production and Operations Symposium, Oklahoma City, OH, USA, 23–25 March 2003.

130. Suarez, L.; Kenyery, F.; Azuaje, M.; Pena, M.A. 3D CFD Simulation of ESP Rotary Gas-Separator Performance Under Two-Phase-Flow Condition. In Proceedings of the SPE Latin American and Caribbean Petroleum Engineering Conference; Intevep: Los Teques, Miranda, Venezuela, 2005.

131. Derakhshan, S.; Riahi, F.; Bashiri, M. Efficiency improvement of a rotary gas separator by parametric study and gas/liquid-flow analysis. *SPE Prod. Oper.* **2018**, *33*, 320–335. [CrossRef]

132. Lackner, G.; Doty, D.; Shirazi, S.; Schmidt, Z. Effect of viscosity on downhole gas separation in a rotary gas separator. *SPE Prod. Facil.* **2002**, *17*, 184–191. [CrossRef]

133. Swetnam, J.; Sackash, M. Performance Review of Tapered Submergible Pumps in the Three Bar Field. *J. Pet. Technol.* **1978**, *30*, 1781–1787. [CrossRef]

134. Camilleri, L.; Segui, E.; Valette, P.; Brunet, L. Poseidon gas handling technology: A case study of two ESP wells in congo. In Proceedings of the Gulf Coast Section Electric Submersible Pump Workshop, Manama, Bahrain, 25–28 September 2011.

135. Lea, J.; Nickens, H.; Wells, M. Chapter 12—Electric Submersible Pumps. In *Gas Well Deliquification*; Gulf Professional Publishing: Burlington, VT, USA, 2003; pp. 239–250.

136. Lea, J.F.; Nickens, H.V.; Wells, M.R. Chapter 12—electric submersible pumps. In *Gas Well Deliquification (Second Edition)*; Lea, J.F., Nickens, H.V., Wells, M.R., Eds.; Gulf Professional Publishing: Burlington, VT, USA, 2008; pp. 361–382.

137. Lea, J.F.; Rowlan, L. 12—Electrical submersible pumps. In *Gas Well Deliquification (Third Edition)*; Lea, J.F., Rowlan, L., Eds.; Gulf Professional Publishing: Burlington, VT, USA, 2019; pp. 237–308.

138. Marsis, E. CFD Simulation and Experimental Testing of Multiphase Flow inside the MVP Electrical Submersible Pump. Ph.D. Thesis, A&M University, College Station, TX, USA, 2012.

139. Hua, G.; Falcone, G.; Teodoriu, C.; Morrison, G. Comparison of multiphase pumping technologies for subsea and downhole applications. In Proceedings of the SPE Annual Technical Conference and Exhibition, Denver, CO, USA, 30 October–2 November 2011.

140. Müller-Link, D.; Rohlfing, G. Grown-up twin-screw multiphase pumps–from marginal to full size applications. In Proceedings of the 14th International Conference on Multiphase Production Technology, Cannes, France, 17–19 June 2009; BHR Group, 2009.

141. MacNeil, D.; Dass, P. Replacing ESP and Gas Lift with ESTSP (Electric Submersible Twin Screw Pumps). In Proceedings of the SPE Artificial Lift Conference and Exhibition, Manama, Bahrain, 27–28 November 2012; Society of Petroleum Engineers, 2012.

142. Centrilift, Inc. *Comparison of Free Gas Handling Abilities of ESP Systems*; Centrilift, lnc.: Claremore, OK, USA; Wharley End, UK; Available online: https://www.wwdmag.com/company/centrilift (accessed on 31 December 2020).

143. Besagni, G.; Inzoli, F. Bubble size distributions and shapes in annular gap bubble column. *Exp. Therm. Fluid Sci.* **2016**, *74*, 27–48. [CrossRef]